

ISO-SWS grating resolution and instrumental profile as measured by the full resolution modes SWS02 and SWS06

Prepared by: D.Lutz, H.Feuchtgruber, J.Morfill

Calibration scientist warning: rebinning is hazardous for the resolution of your SWS data!

1	Introduction	2
2	Spectral resolution	3
2.1	Cautionary note: The effects of rebinning	3
2.2	Existing models for the SWS spectral resolution	3
2.3	Description of the database	5
2.4	Resolution for sources of different size: Observations and simple model	9
2.5	Dependence of resolution on line flux or continuum flux?	16
2.6	Reproducibility and trends with time	16
2.7	Variation among detectors	17
3	Line profile asymmetries and deviations from gaussian shape	21
3.1	Reference quantities for an intrinsically gaussian line	22
3.2	The SWS profiles	23
3.3	Probing the mud: Line profiles below 1% of the peak height	27
3.4	Search for ghosts	31
4	The effects of mispointing: A test	32
4.1	Wavelength shifts	34
4.2	Resolution	34
4.3	Profile shapes	36
5	Detector transients: Effects on Line profile	39

6 Appendix: Description of CAP 6.3.2.1	43
6.1 C321_LINES.PRO	44
6.2 Emission lines used for line profile determination	46
6.3 Sources used for line profile determination	46

1 Introduction

This document presents an empirical overview of spectral resolution and line profile properties for the full resolution modes of the ISO-SWS grating spectrometers (SWS02, SWS06). For any spectrometer, these are among the instrument characteristics most directly related to the interpretation of scientific data. For SWS, users have up to now mostly relied on a software module (**RESOLUTION**) in the SWS interactive analysis system (IA), which implements a simple model of SWS geometry and diffraction, and on plots in the SWS observer's manual ([Leech et al. 1996]) which were derived on the basis of an earlier version of that model. Note that results for extended sources differ between these two references. For a single almost pointlike source, these assumptions were found to be valid ([Valentijn et al. 1996]). A first more comprehensive report on the performance measured in orbit ([van den Ancker et al. 1997], see also the SWS IDUM [Leech et al. 1997]) suggested that expected and measured spectral resolution are in conflict, especially for extended sources.

The SWS In Orbit Calibration Document (IOCD, [Valentijn et al. 1995]) called for a more ambitious program of establishing and evaluating a database of measured line profiles (Requirements 6.3.2.1 Grating Instrumental Profile (IP) - Point source and 6.3.2.2 Grating Instrumental Profile (IP) - Extended source). This is what we are pursuing here, based on a significant part of the suitable SWS observations. Only a wider empirical basis, analysed in a homogeneous and systematic manner, can tell to which extent the mentioned discrepancies persist, and whether the widely used resolution model has to be revised.

Of the three SWS grating observing modes, we limit ourselves to the SWS02 mode which reproduces the intrinsic resolution of SWS and ensures a dense sampling of the line profiles. The SWS01 mode introduces an additional smoothing which, due to the intricacies of SWS data acquisition, is different from a simple boxcar smooth. However, the result can now be well modelled given a good intrinsic line profile [Lorente 1998]. Like SWS02, the SWS06 mode in principle reproduces the full intrinsic resolution since the grating does not move during a reset interval. It is mostly applied, however, to cover larger ranges within the available time, which leads to poorer sampling of the line profile by a single detector. For the purpose of derivation of high fidelity line profiles, this causes unwanted interactions between the line profiles and the relative sensitivities of the 12 detectors of a band ('flat-fielding' in SWS-speak), since all twelve detectors have to be combined for a good profile. This is our reason for preferring the SWS02 mode where already single detector profiles are well sampled and can be combined with much less danger of introducing artefacts. An obvious corollary of this approach is that we make only a very limited attempt (Section 3.3) to probe for the line profile behaviour on larger scales than a few times the FWHM, since they are not well covered by SWS02. As discussed below, the only significant effects on that scale are related to memory effects in band 2 and 4.

In principle, any SWS02 observation is suitable for line profile determination, given that

- The line is detected with adequate signal-to-noise

- The line is on a clean continuum and free of nearby satellites. Here, compromises have to be taken since a fringy band 3 continuum will never be perfect. Also, we use for example simple resolution values measured on H recombination lines, despite knowing that the lines are disturbed at a lower level by Helium satellites. This is evident in many ISO data, like those of [Rubin et al. 1998].
- The spatial structure of the source is known. This is important since, like for many spectrometers, a point source does not fill the SWS slit. The resolution for a perfect extended source should hence be somewhat lower than for a perfect point source.
- The intrinsic width of the emission line is either in the range of 50 km/s FWHM and reasonably well known, or significantly lower. Because the SWS resolution exceeds 2000 over wide ranges, even such relatively narrow intrinsic line widths will already significantly widen the observed line profile. This excludes for example all extragalactic sources despite being often favourable close to pointlike for SWS spatial scales.

Since these criteria will never be met to 100% in practice for a single source, and since pointing uncertainties may introduce further scatter, we have chosen an approach of building up a database that may help in catching rogue observations.

2 Spectral resolution

2.1 Cautionary note: The effects of rebinning

It should be emphasized that *all resolution values quoted in the remainder of this document refer to the intrinsic resolution as measured by gaussfits to the AAR ‘dot cloud’*. However, essentially all SWS data reduction recipes involve a step of ‘rebinning’ or ‘convolution’ aiming at collapsing the dot cloud into a single valued spectrum. Necessarily, this has an effect on the resolution measured in the final spectrum whose magnitude sensitively depends on the chosen parameters. Since, for good reasons, different routines and widely varying parameters are chosen, by different users and for different projects, no general ‘resolution’ can be quoted for a rebinned spectrum.

Users who need accurate linewidths from rebinned spectra should estimate this effect themselves for the exact parameter combination adopted in their data reduction. Just as an illustrative example, we show in Figure 1 and Table 1 the effect of using the IA **SWS_REBIN** and **AARFILT** modules on a strong [Ne III] line. It should be noted that the relatively low ‘resolutions’ often used in rebinning for S/N reasons significantly affect line profiles.

2.2 Existing models for the SWS spectral resolution

Because of considerable confusion on what the ‘expected’ spectral resolution of SWS is, we give a short summary of the various models available. This is largely based on an E-mail by Edwin Valentjin (4.11.1998). There are three different flavours which we will call model 1 to 3. They are described below and the resulting resolutions summarized in Figures 2 and 3.

- Model 1: This is a MIDAS-based version used for the FM-ILT reports and the Observer’s manual [Leech et al. 1996]. Good agreement between this model and the laboratory solid state

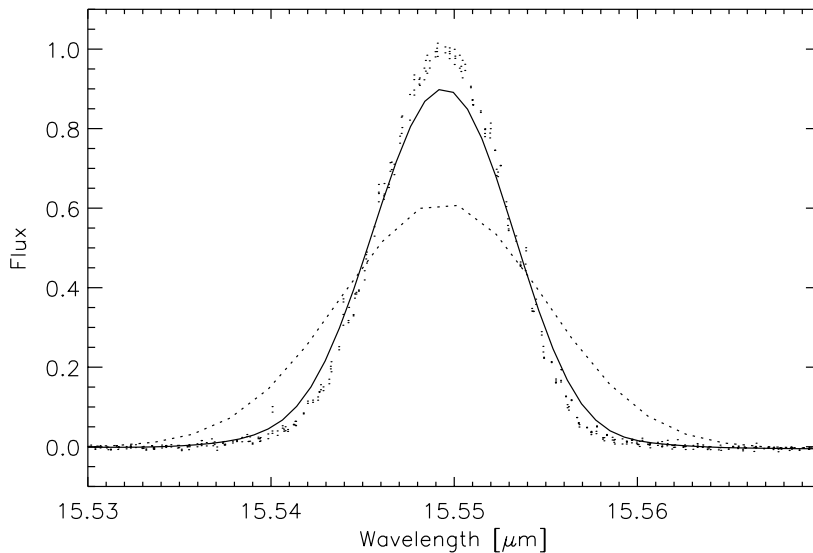


Figure 1: Effect of rebinning on a SWS line profile. The chosen example is a [NeIII] line with the original data shown as dots. The continuous line is the result of rebinning like `aar=sws_rebin(ne3,resolution=4000,over=5,/noplot)` and the dotted line of rebinning in the same spirit using resolution 1500, which is the `sws_rebin` default for AOT SWS02. The profile changes considerably.

Filter	Measured SWS_REBIN	Measured AARFILT
No	(1936)	(1936)
10000	1903	1920
5000	1811	1869
3000	1633	1801
2000	1395	1730
1500	1188	1708
1000	891	1303

Table 1: The effect of rebinning on the spectral resolution of SWS data: Resolutions measured by gaussian fit to original and rebinned data of the example line shown in Figure 1. The IA syntax used for rebinning was like `aar=sws_rebin(ne3,resolution=5000,over=5,/noplot)` and `aar=aarfilt(ne3,[15,16],5000,kappa=2.5)`. Note that there is an additional default convolution in `SWS_REBIN` unless switched off, and a clipping in `AARFILT`. If both are suppressed, results from the two modules are very similar.

laser experiments (extended source!) is stated there. Note that no crosstalk corrections were applied to the data at this time.

- Model 2: This is the current IA RESOLUTION module (Version 2.5) used with default detsize parameter. [Valentijn et al. 1996] state excellent agreement to a few percent between this model and the very compact planetary IC 2501, whereas [van den Ancker et al. 1997] find discrepancies between this model and observations. Model 2 differs from model 1 in a different treatment of diffraction.
- Model 3: The default detsize values in IA RESOLUTION assume that the detector size is equal to the spacing between detector centers. This is correct for the band 3 BIBIBs but not for the other bands which have small gaps between the detectors. The detsize values recommended by E. Valentijn (0.0168271, 0.0188922, 0.0314100 for bands 1,2, and 4, priv. comm.) have been used for model 3. Model 3 is supposed to be the best according to knowledge previous to this investigation.

The differences between the various models are nonnegligible, which means that the good agreement found with different models in different situations indicates a problem in understanding the SWS resolution. In the following, we will proceed with the empirically measured resolutions, but use model 3 as the comparison where appropriate.

2.3 Description of the database

Our database contains a significant variety of source types: planets, HII regions, planetary nebulae, PDRs. The basic assumption is that each source can be described by a single diameter, a single gaussian FWHM line width, and a radial velocity. Of course, this assumption is not really correct for diameter and line width: The diameter of an ionized nebula will usually be larger in low ionization species or molecules than in high ionization ones, and because of the different thermal broadening H lines will be broader than fine structure line. The unavailability of detailed data for most lines/sources forces us, however, to stick to the simplifying assumptions. Only in very few cases (e.g. size of NGC7027 in H₂ vs. ionized lines) we have made use of better constraints and deviated from these assumptions. Mid-infrared emission line maps for some of the planetary nebulae used in this study have recently been published [Persi et al. 1999]. The measured emission line sizes are in very satisfactory agreement with our adopted values for the sources and lines in common. The striking difference in their [NeII] and [NeV] images of NGC 6720 (not used here) cautions again that a single source diameter is a simplification.

To derive the true resolving power of SWS it is mandatory to correct for the line width of the sources. This is especially relevant for the planetary nebulae which typically show line widths of the order 40km/s. The effect has, however, not been taken into account in previous analyses. Since the SWS lineprofiles are close to gaussian, we assume that line widths can be subtracted in quadrature. For example, assuming measured R=2500 as reached over a significant part of the SWS range, and a line width of 40km/s, the true resolution after correction would be about 2650. Figure 4 shows examples of this correction factors for some real data.

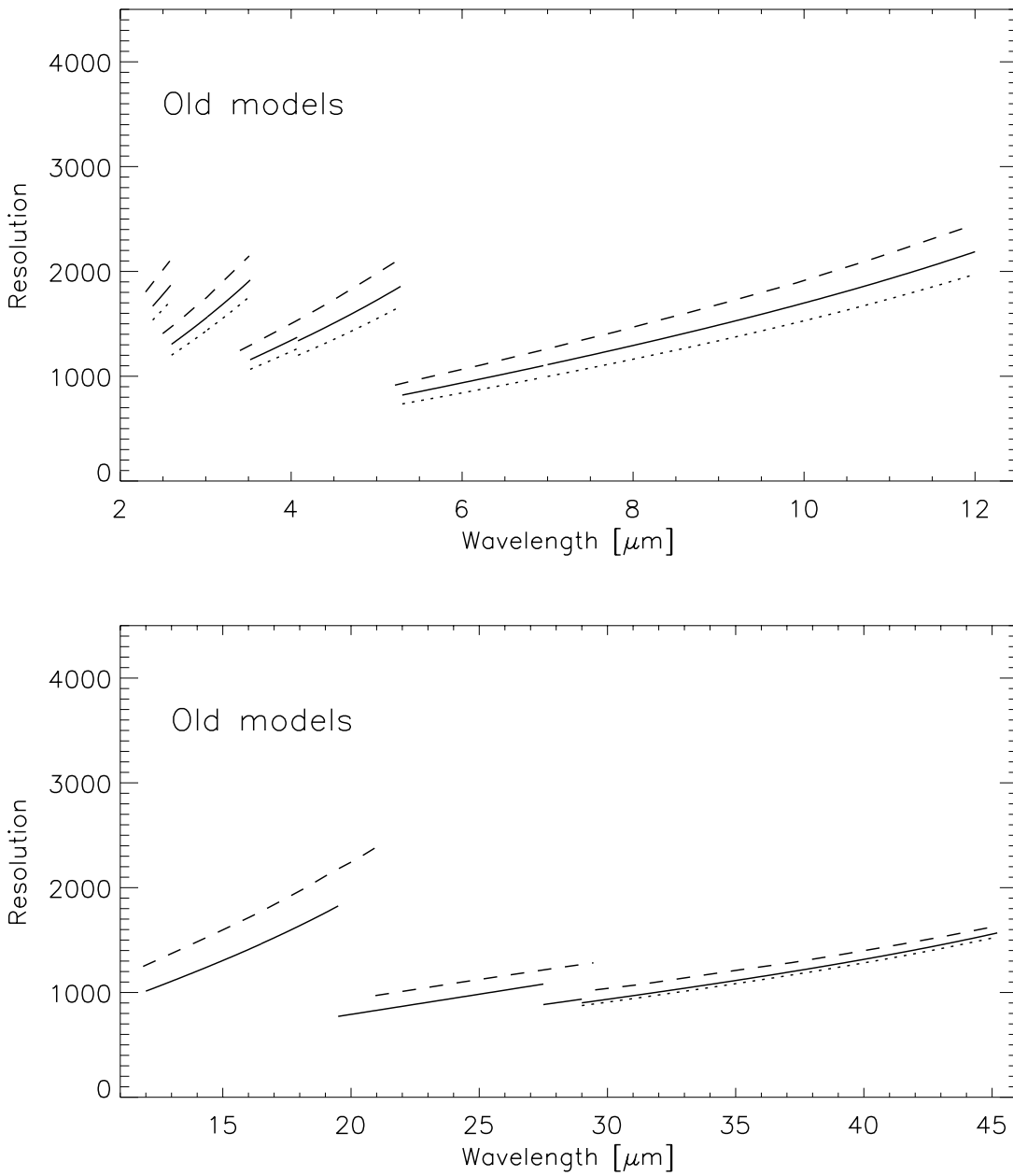


Figure 2: Expected spectral resolution of SWS for an extended source, based on the three models described in the text. Model 1 (dashed) is the pre-launch version as printed in the Observer's manual. Model 2 (dotted) is the current IA **RESOLUTION** module (Version 2.5) with default detsize value. Model 3 (continuous) is the model recommended previous to this work, which is IA **RESOLUTION** with more appropriate detsize values. For band 3, there is no difference between models 2 and 3, since there are no spaces between detectors. Note that there were also changes in AOT band limits between model 1 and the others.

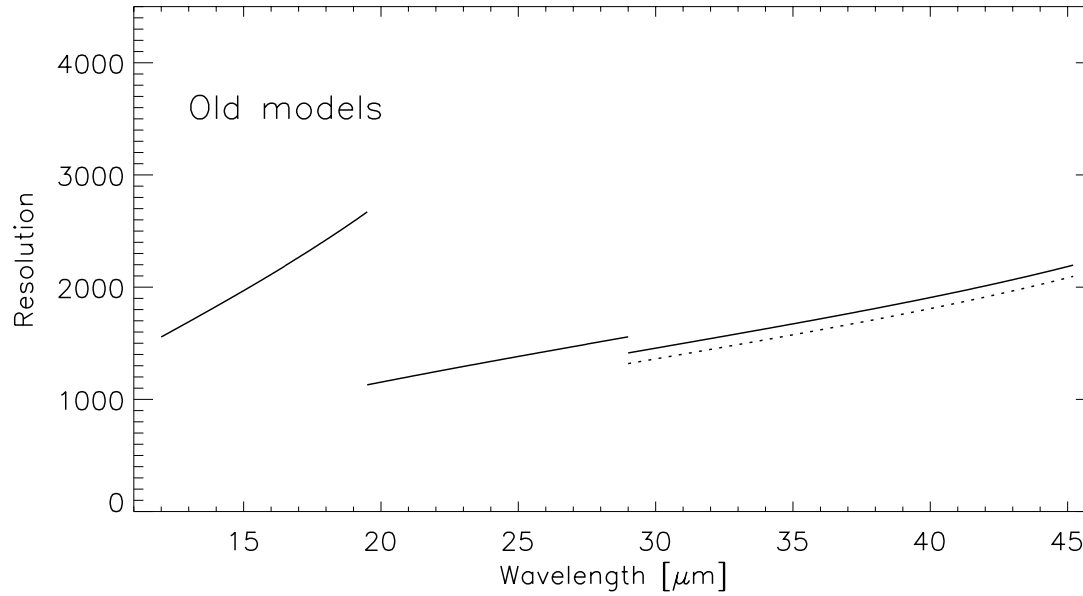
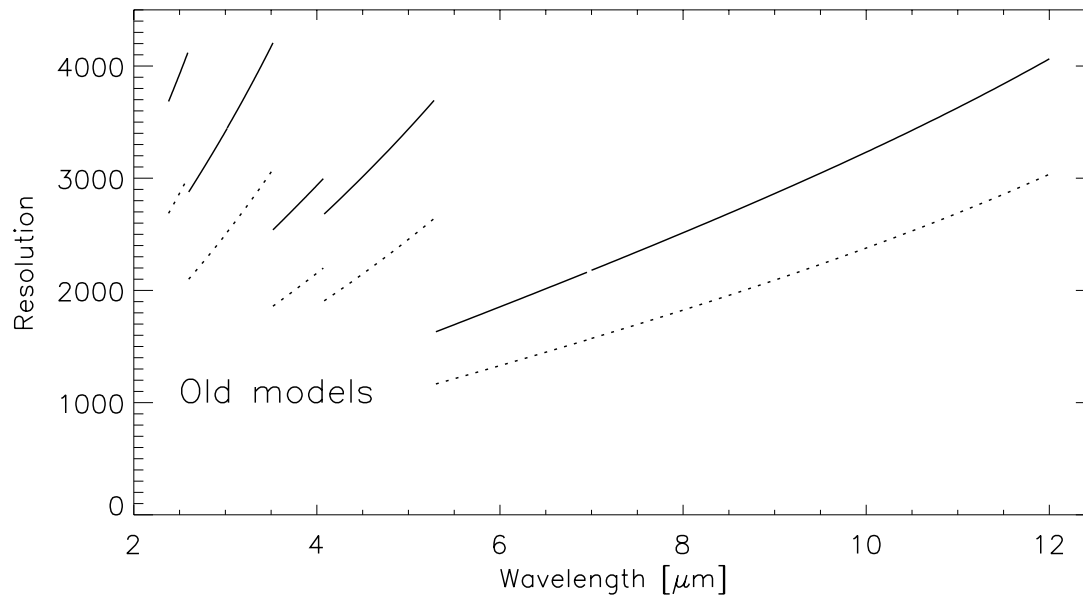


Figure 3: Expected spectral resolution of SWS for a point source, based on models 2 and 3 described in the text. Model 2 (dotted) is the current IA RESOLUTION module with default detsize value. Model 3 (continuous) is the model recommended previous to this work, which is IA RESOLUTION with more appropriate detsize values.

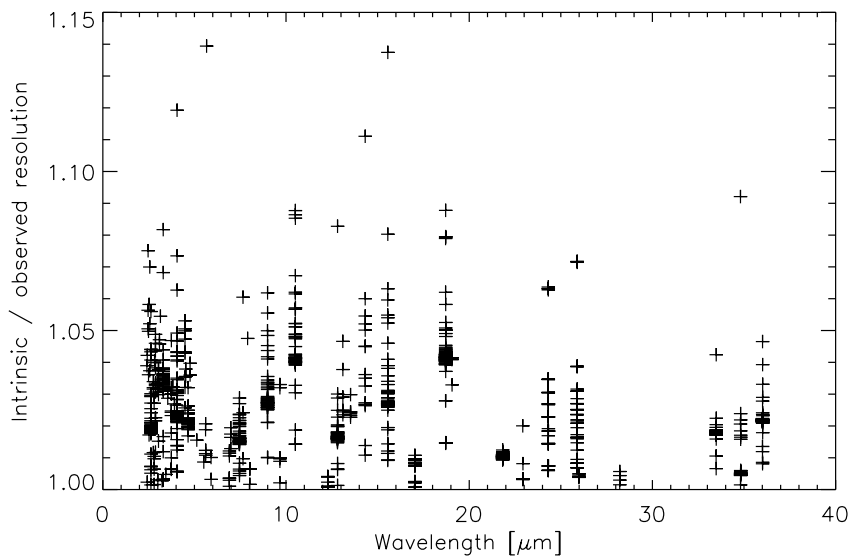


Figure 4: Effect of intrinsic source line width on the derived SWS resolution: The ratio of intrinsic (i.e. corrected) SWS resolving power to directly observed resolving power is plotted for a large part of the database containing both PDRs with narrow lines ($\text{FWHM} < 20\text{km/s}$) and planetary nebulae with somewhat wider lines (up to 80km/s). Corrections are small for the PDRs but reach 5% for a significant part of the SWS range even for moderate velocity width planetary nebulae.

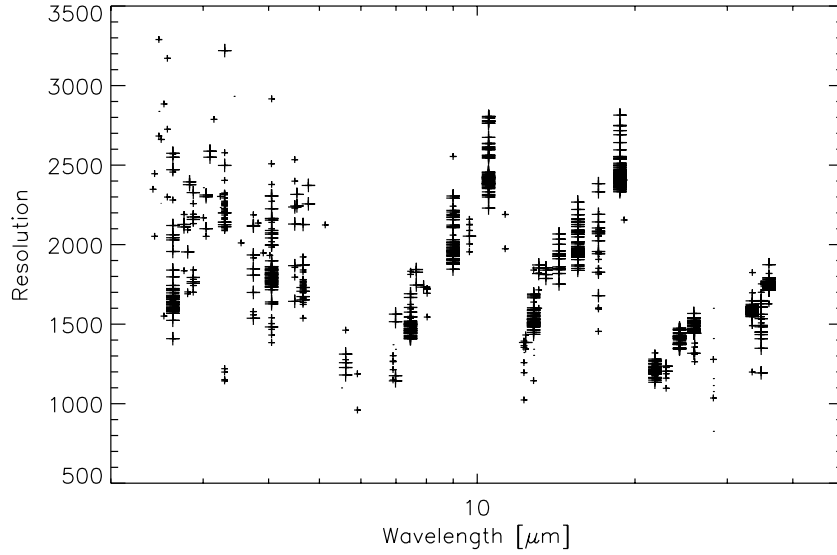


Figure 5: Summary of measured SWS spectral resolutions, including all sources and lines irrespective of source size and S/N. Symbols of different size reflect data of different S/N.

2.4 Resolution for sources of different size: Observations and simple model

All measured SWS resolutions, corrected for the intrinsic linewidth, are shown in Figure 5. The figure is quite crowded, including a wide mix of sources. A few facts are already obvious: At a given wavelength beyond $10\mu\text{m}$, the spread in measured resolutions is small. This indicates immediately that the difference between resolution for point and extended sources cannot be large, although its signature is evident on detailed inspection: lines like H₂ S(1) for which several very extended sources could be analysed tend to return lower resolution than the fine structure lines observed mainly in planetary nebulae of various sizes.

The trend of resolution with source size is better demonstrated in Figures 6 and 7 which show the measured resolution as a function of source diameter for a number of bright lines. The expectations for point and fully extended sources from model 3 are included as dotted lines. These expectations fit quite well at the shortest wavelengths, e.g. for Brackett β . In contrast, the measured resolutions are significantly better than expected from model 3 for long wavelength lines. This difference is strongest for large sources and smaller but still present for pointlike source. As a consequence, the resolution spread between different source sizes is reduced strongly.

No good model explaining the measurements from first principles is currently available. It should be noted that, if the resolution is affected by blue wings of unclear origin (Sections 3, 4.3), then a good model of this type will be difficult to obtain. We have hence chosen the approach of fitting a simple function to the measurements, to provide a fully empirical model of the SWS resolution that will be suitable for most practical purposes. The choice of function is motivated by the following reasons:

- Unlike the spectral resolution, the line FWHM in μm varies little over an AOT band. It is hence preferable to fit the FWHM, allowing at most a linear variation with wavelength, and later convert to resolution.
- For very small sources, the resolution should be independent of size since diffraction by the ISO telescope will dominate the width of the profile entering the SWS slit. The definition of ‘very small’ will vary with diffraction i.e. with wavelength.
- For very large sources, much larger than the SWS slits, the resolution will again be constant.

We have made the following **AD HOC** choice for fitting the FWHM values measured within an AOT band, assuming a source of diameter d arcsec observed at wavelength $\lambda \mu\text{m}$:

$$FWHM(d, \lambda) = c_1 + c_2\lambda + c_3\tanh(c_4(\log_{10}(d) - c_5))$$

The tanh function does not reflect a physical model. Its choice is simply motivated by having the proper asymptotic behaviour, and by providing an acceptable fit. No automatic least squares fit was attempted, since some AOT bands are poorly sampled, and since there is a significant number of outliers. The best fit values listed in Table 2 result from a software tool which allows to vary the parameters of this function and compare results to data for a single AOT band. The quality of the fit is judged by eye, first using the smallest and largest source data to fix c_1 and c_3 , and then choosing c_4 and c_5 to fit intermediate data. A nonzero c_2 is only required for the long AOT band 2C. Poor sampling of wavelength space by bright lines makes c_2 impossible to determine reliably for other bands. In fitting the various AOT bands, we also considered continuity of fit parameters at band limits where

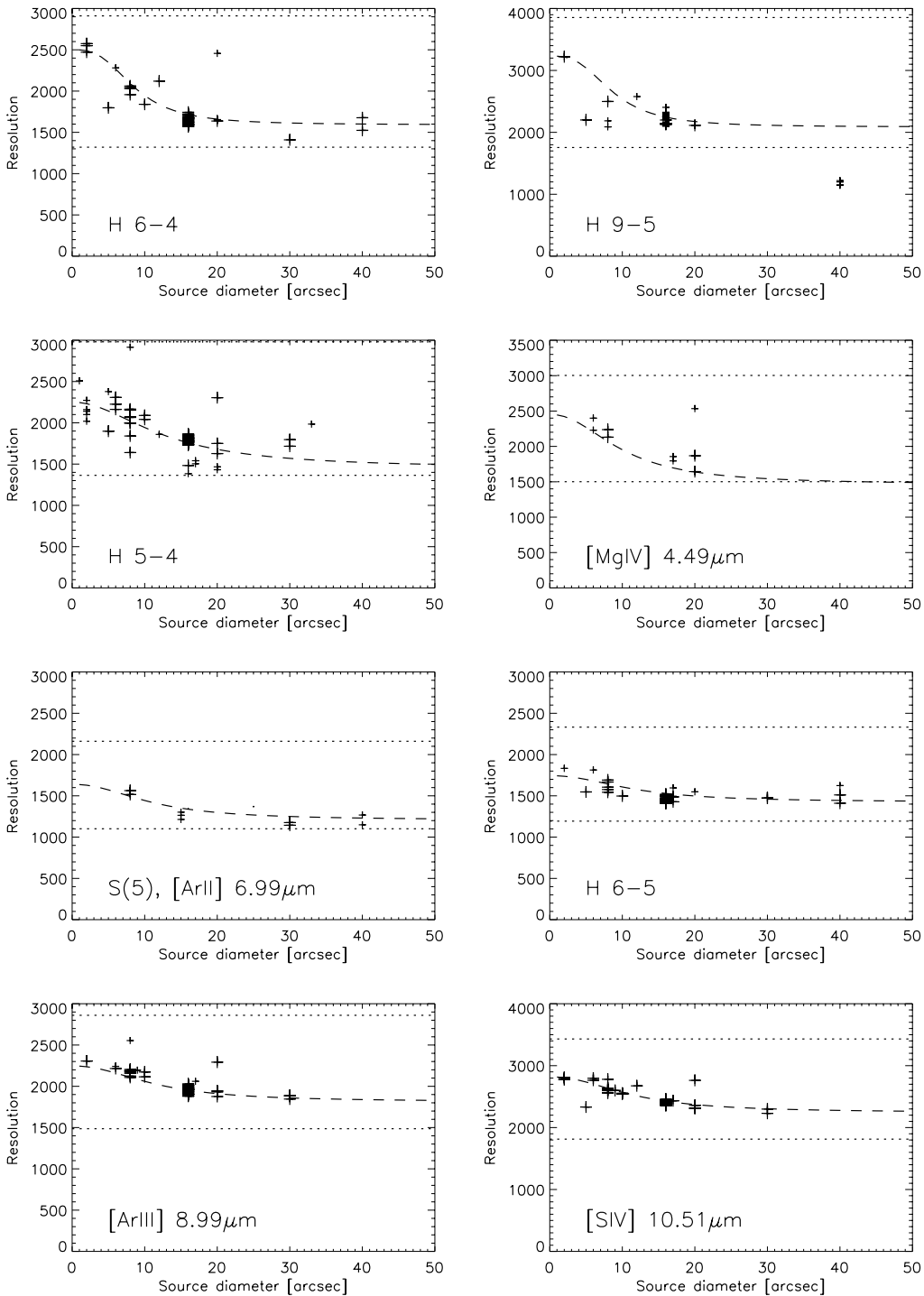


Figure 6: Resolution as a function of source diameter, for several bright lines in the SW section of SWS. Symbols of different size reflect data of different S/N. The data at (formal) diameter 40 arcsec represent several regions that are much larger than the SWS beam but structured, so that each individual measurement may be centered on a knot or gap causing scatter in the expected resolution. The dotted lines are the model 3 values for point and extended source. The dashed lines are the predictions from the **preliminary** empirical model described in the text and in Table 2.

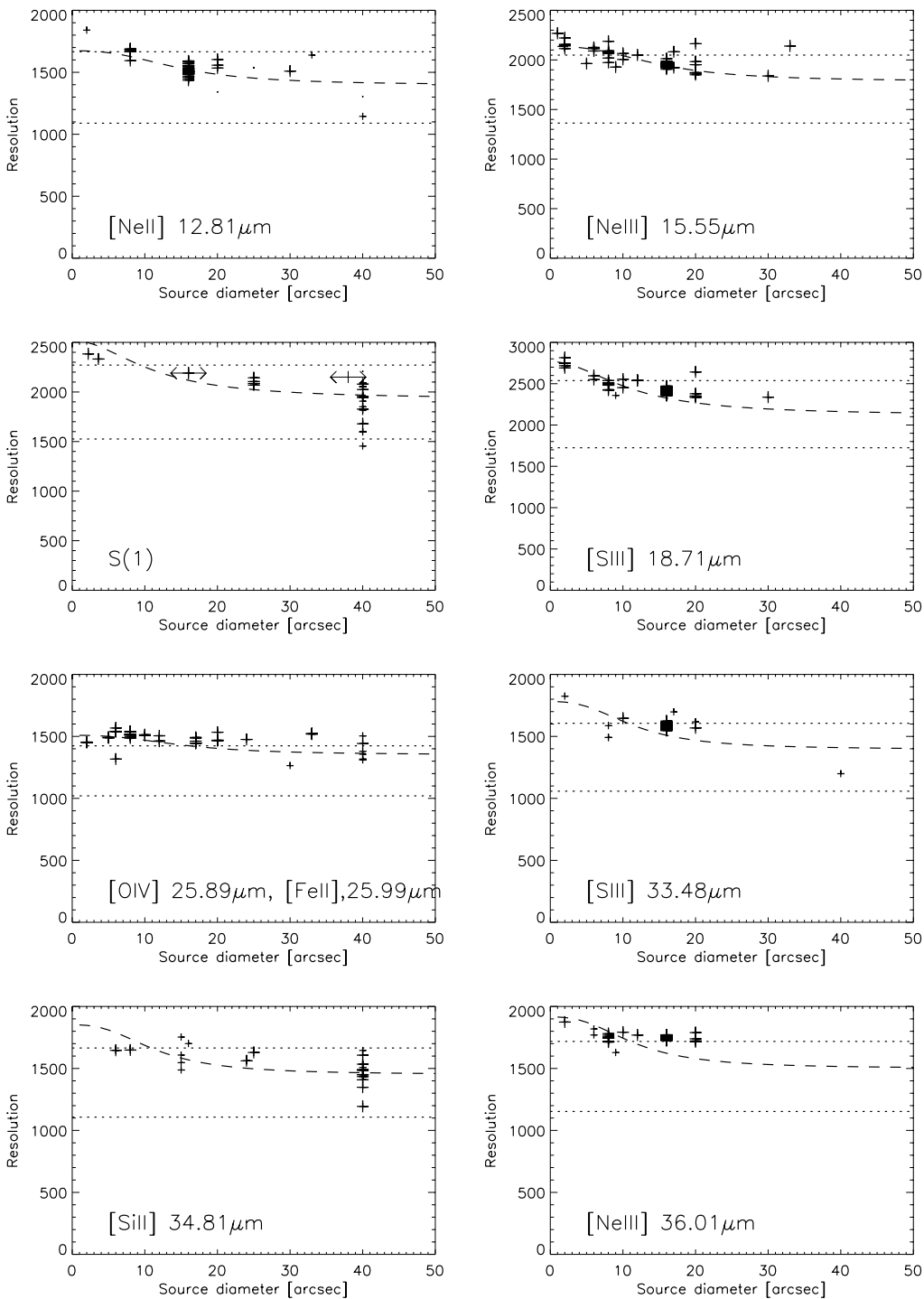


Figure 7: Analogous to Figure 6. Resolution as a function of source diameter, for several bright lines in the LW section

AOT band	c ₁	c ₂	c ₃	c ₄	c ₅	Comments
1A	0.00095		0.00026	3.40	1.00	
1B	0.00135		0.00030	3.40	1.00	
1D	0.00130		0.00028	3.40	1.00	
1E	0.00230		0.00050	2.30	1.20	
2A	0.00245		0.00062	2.50	1.10	
2B	0.00500		0.00076	2.50	1.10	
2C	0.00610	-0.00018	0.00048	2.50	1.10	
3A	0.00820		0.00105	3.00	1.20	
3C	0.00780		0.00104	2.30	1.10	
3D	0.01830		0.00120	3.00	1.20	
3E	0.02010		0.00220	3.00	1.10	Guess!
4	0.02140		0.00260	3.00	1.10	

Table 2: Fit coefficients for the simple empirical model fitting the SWS instrumental profile FWHM as a function of source size and wavelength. See text for details of the fit function.

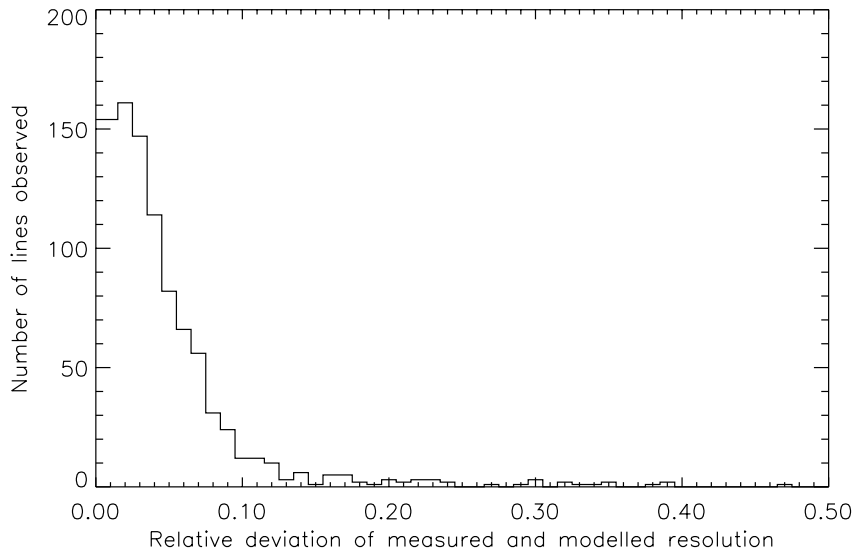


Figure 8: Histogram of the relative deviation between observed resolution and resolution derived on the basis of the simple empirical model, for all lines in our database.

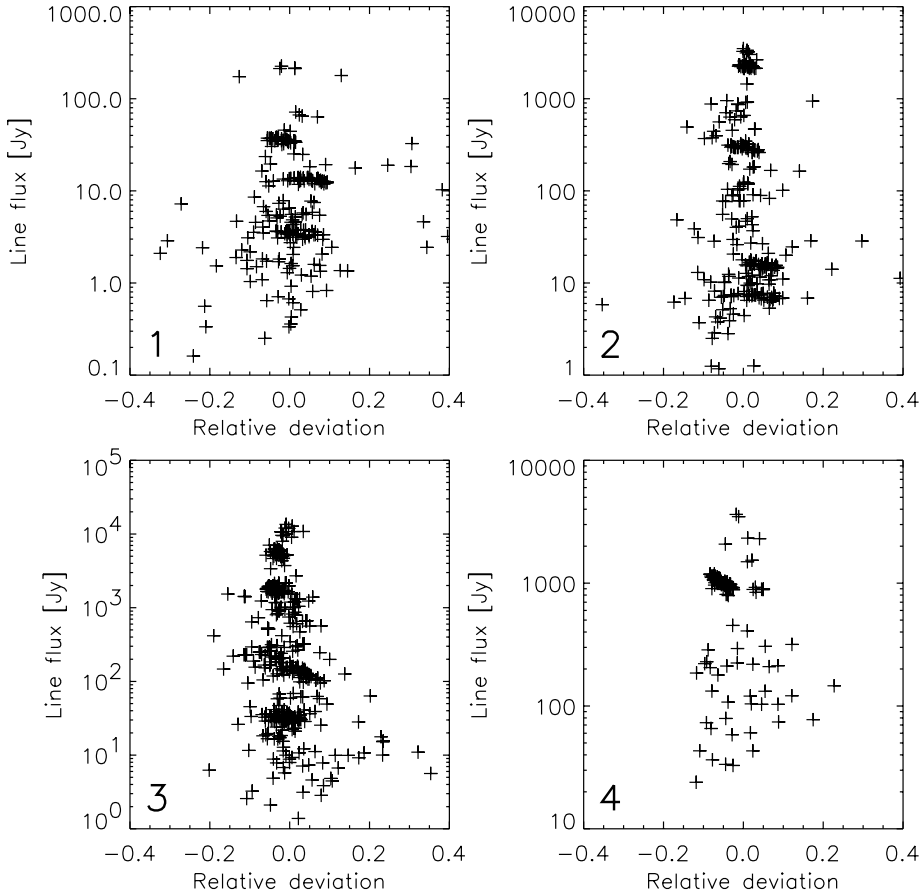


Figure 9: Relative deviation between observed resolution and resolution derived on the basis of the simple empirical model, as a function of line flux. The four SWS bands are shown separately. The tilted sub-clouds of measurements can be easily explained as due to many repeated observations of NGC 6543, with flux and resolution varying as the slit rotates (see also section 2.6). There is no indication for a flux dependency of resolution.

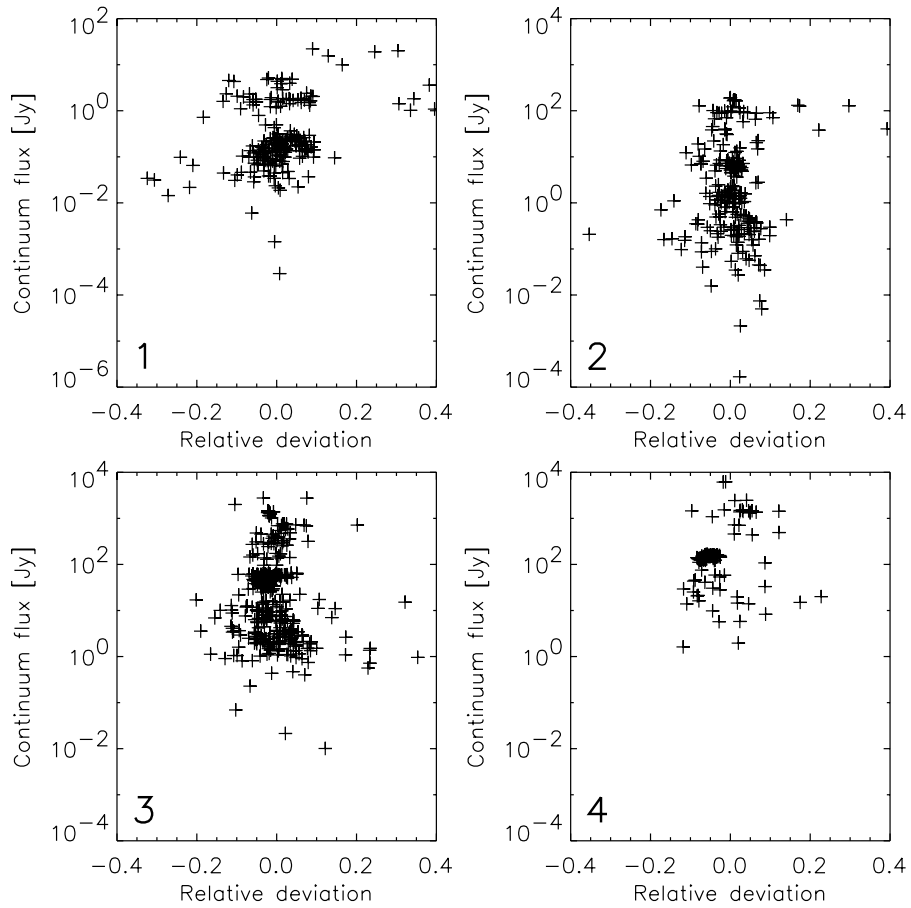


Figure 10: Relative deviation between observed resolution and resolution derived on the basis of the simple empirical model, as a function of continuum flux. The four SWS bands are shown separately.

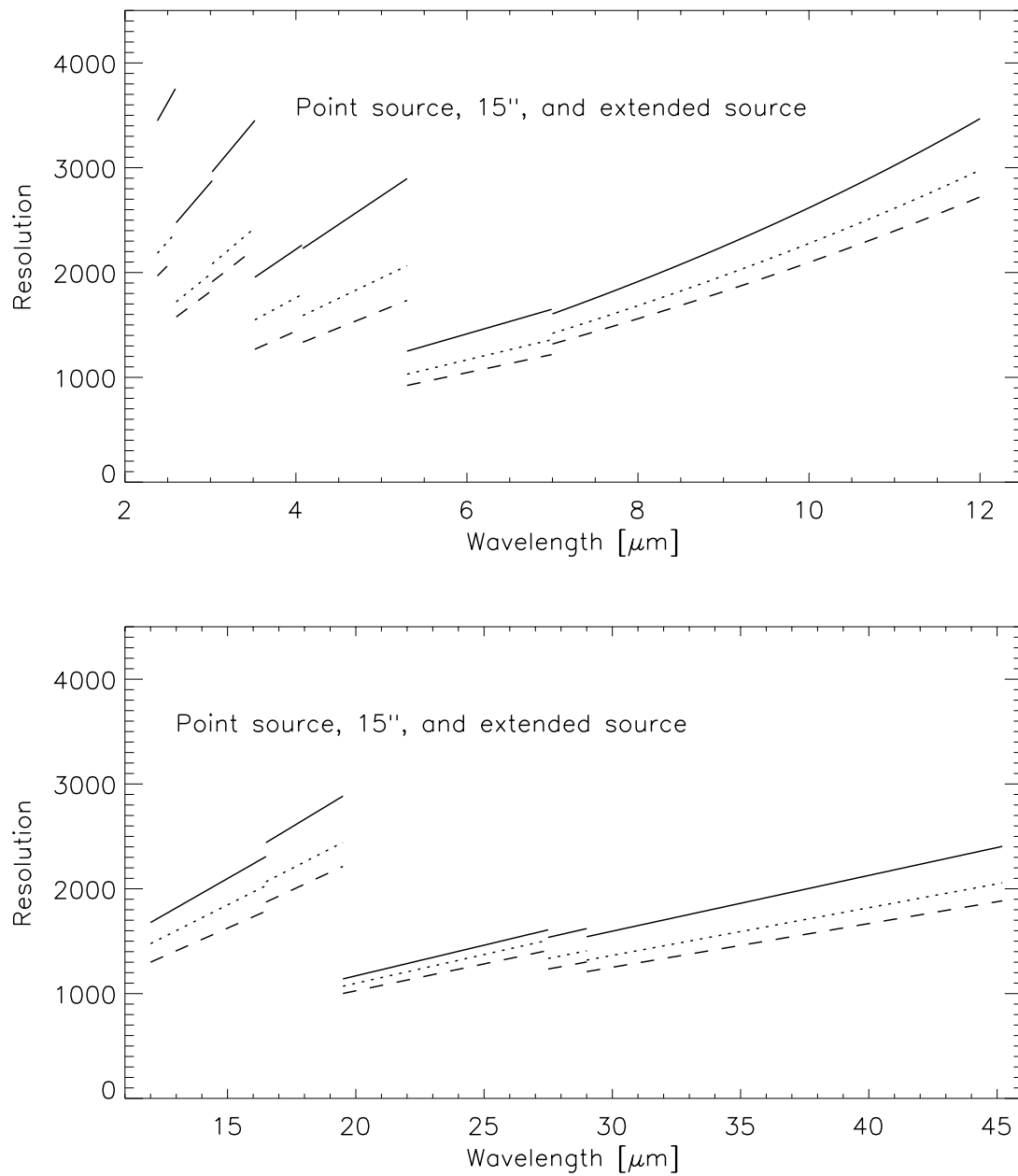


Figure 11: Spectral resolution of SWS for a point source (continuous), a 15'' diameter source and a fully extended source as predicted from the new empirical model

it should exist. The fit parameters listed in Table 2 hence are the result of a best effort but subjective procedure.

Resolution as computed from the new empirical model is visualized in Figure 11. We estimate that the empirical model fits the true SWS resolution to an accuracy of about 10% overall. Figure 8 might suggest at first glance an even better accuracy, since essentially all measurements are within less than 10% from the model so that the ‘mean’ of various scattering measurements should be even better defined. The 10% estimate tries to incorporate various remaining systematic uncertainties: The emission line data do not sample the parameter space evenly. They are deficient in some bands or towards edges (e.g. for band 4 where only the region around $35\mu\text{m}$ is covered well). Also, most sources are of intermediate diameter while point sources and very large sources are few. There will be residual problems with velocity widths and diameters assigned to sources. Necessarily, such a simple empirical model will hence be best near bright lines and for sources of intermediate diameter (5-20arcsec). Results are relatively uncertain for very large sources. For the molecular hydrogen S(1) line, for example, the most reliable large source is Jupiter which gives a relative high resolution. Lower resolution is suggested by some molecular clouds near the center of our galaxy but may be affected by highly uncertain intrinsic velocity widths. We have not clearly preferred one or the other option, but rather adopted an intermediate resolution for ‘large’ sources.

2.5 Dependence of resolution on line flux or continuum flux?

For detectors that are nonlinear due to e.g. transients, a dependence of spectral resolving power on flux cannot be excluded in principle. While transients affect the faint wings of some SWS lines (see below), no effect is noticeable in practice for FWHM and resolving power. This is demonstrated in Figures 9 and 10. Since it is impossible to find reliable ‘matched pairs’ of bright and faint sources with identical spatial structure and velocity width, we plot again a comparison of observed and modelled resolution for our entire sample. The observed resolution has been corrected for intrinsic velocity width, and the modelled one is based on the simple empirical model which considers wavelength and source size. Figures 9 and 10 plot the deviation of observation and model as a function of line flux and continuum flux. Except for increased scatter for faint sources, no systematic trends with flux are visible, to a level of a few percent. The diagrams contain some conspicuously tilted sub-clouds of measurements which, however, can be easily explained as due to many repeated observations of NGC 6543, with flux and resolution varying as the slit rotates (see also section 2.6 below).

2.6 Reproducibility and trends with time

The bright planetary nebula NGC6543, placed in the zone of permanent visibility close to the ecliptic pole, was observed with SWS more often than any other emission line source, and is uniquely suited to test the stability of the instrumental profile. Figures 12 and 13 show how the measured resolution (normalized to its median over time) changes for various measurements. While there is scatter at the 5% level for some of the fainter lines (which however still are high S/N detections), the very bright lines are extremely stable with no trend over the 2.5 years of the mission. The only significant variation is a semi-annual modulation of the resolution seen most clearly in the low excitation lines arising in the outer regions of the nebula. This is very likely caused by the slit being sometimes aligned and sometimes non-aligned with the slightly elongated nebula as the ISO sun constraint forces the ISO attitude to change. Periodic shifts of the line with respect to fringe patterns could cause

similar modulations. They should however be annual, and probably less well phased than observed here. Also, no variations would be expected for the band 4 line of [SIII].

The line profile parameters seem to be stable, with the possible exception of a small semi-annual modulation of the line centroids at low level (TBC), which might be related to the blue asymmetry.

A quick inspection of measured wavelengths suggests for some lines small residuals (few 10 km/s) due to the finite periods in the timedependency of the wavelength calibration (Calibration files as of OLP 7.0).

2.7 Variation among detectors

For bright lines, CAP 6.3.2.1 returns line FWHMs for the individual detectors as well as for the combined array. Figure 14 compares them for all lines which were bright enough to return detector specific FWHM values for all detectors of the array. There are some obvious variations reaching 10% in the most extreme cases. The SWS02 data are not ideally suited for this investigation since, for most wavelengths, the edge detectors will see continuum on one side of the line only. The FWHM values for the edge detectors may hence be less accurate. At least for band 4, however, the scan range is large enough to make such problems very unlikely.

The reason for these variations is not understood at the moment - several different influences might be involved (effective detector sizes taking into account sensitivity variations, optical reflections, electrical crosstalk etc.). A practical consequence is that in reductions which discard data for some detectors (as common for band 3), very small resolution variations of the order % might arise, depending on which detectors are discarded.

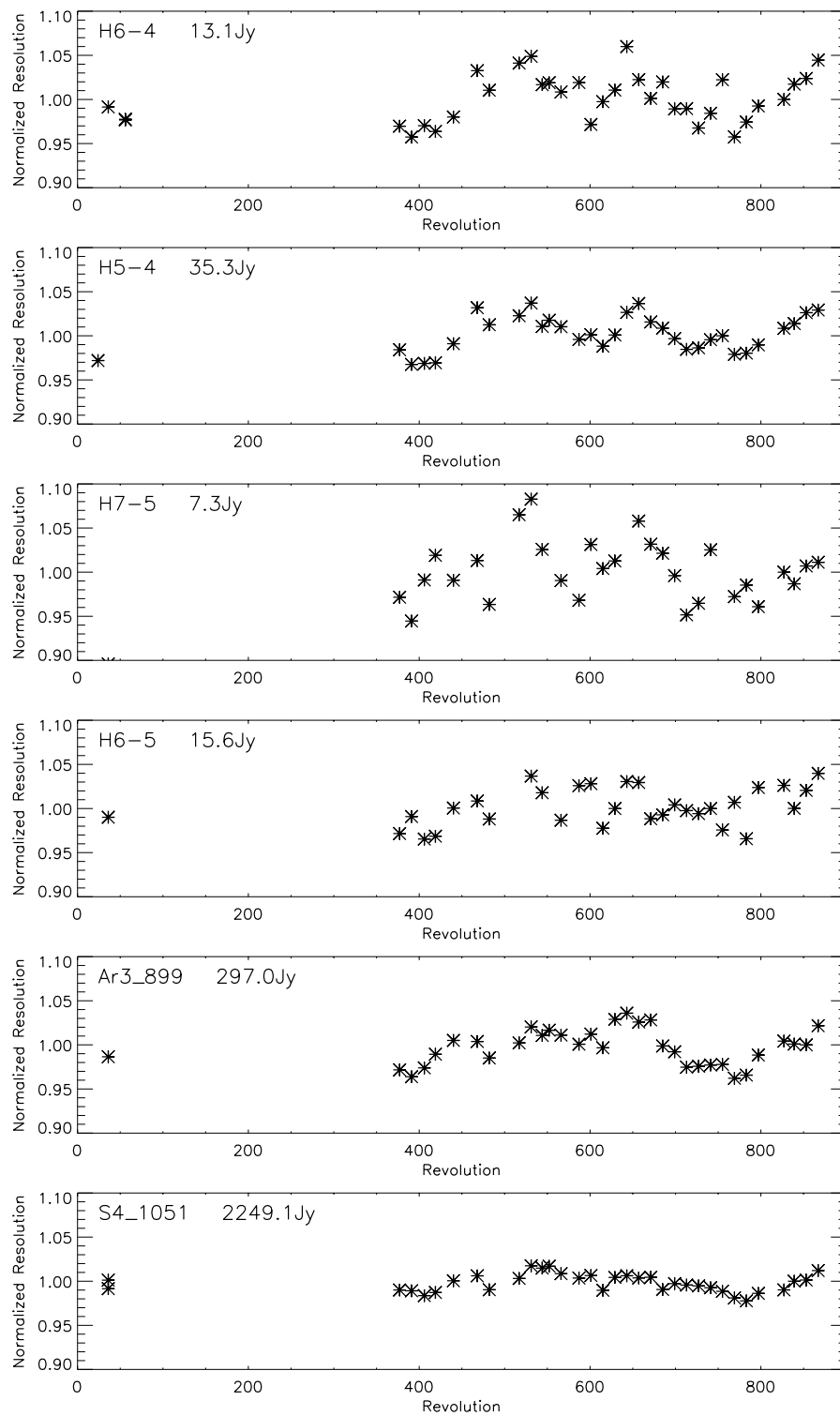


Figure 12: Resolution measured over the ~ 900 revolutions of the ISO mission for various emission lines in the planetary nebula NGC 6543

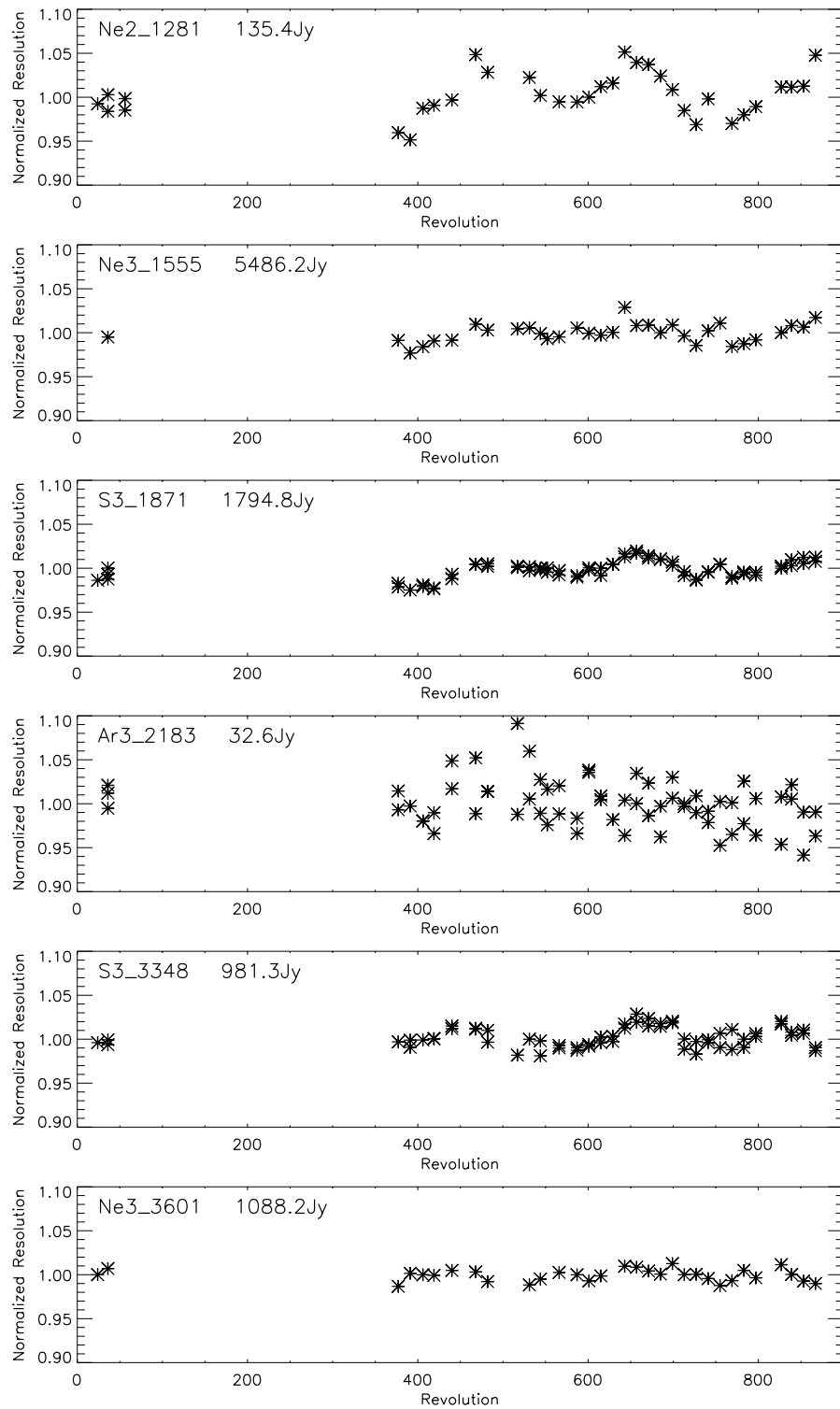


Figure 13: Resolution measured over the ~ 900 revolutions of the ISO mission for another set of emission lines in the planetary nebula NGC 6543

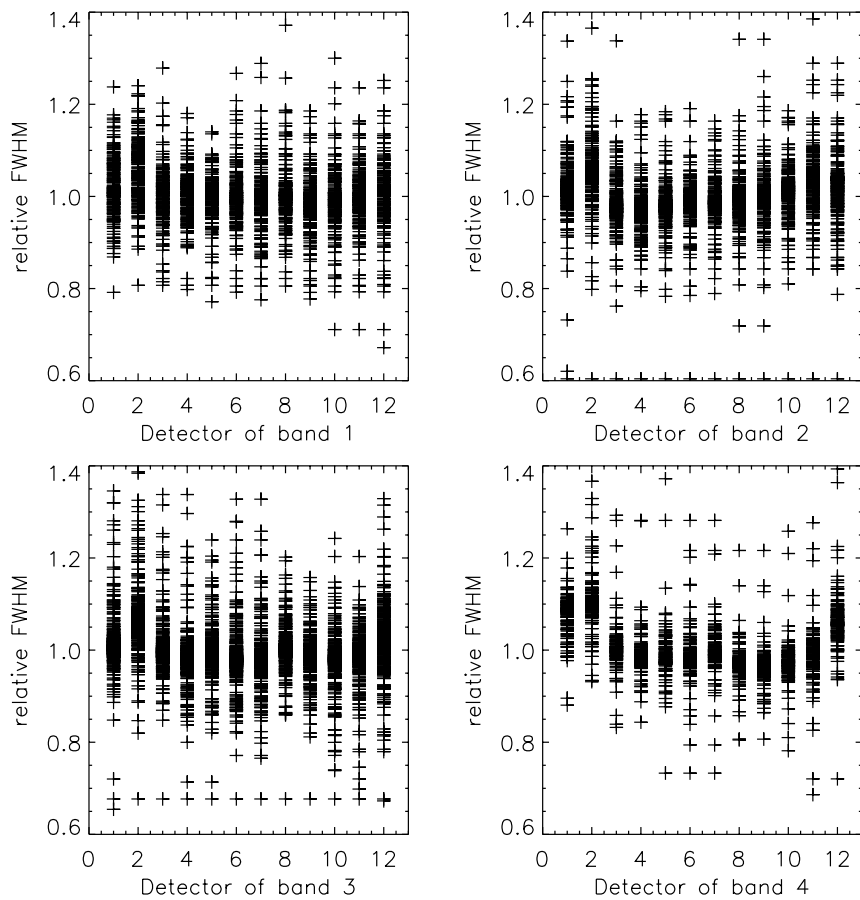


Figure 14: Resolution measured with individual detectors normalized to resolution measured with the entire array. Some, but perhaps not all, of the variations seen are real (see text)

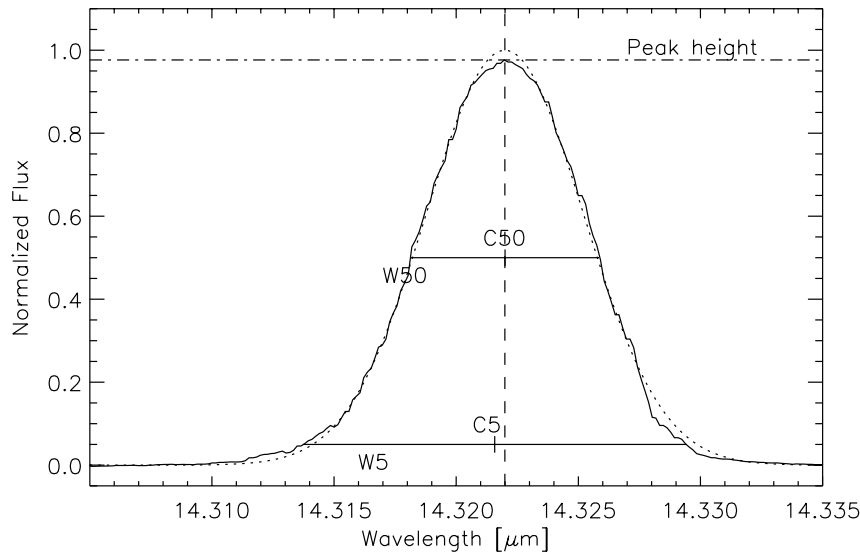


Figure 15: Examples of line profile parametrizations used in this document. The continuous line is the average rebinned profile of the [Ne V] line in NGC 7027, the dotted line is a gaussfit to the original dot cloud. CXX and WXX are the line centroid and width of the average profile at a height of XX% of the peak height of the gaussfit to the original dot cloud. They are given in units of the gaussfit FWHM and relative to the gaussfit center. The peak height of the average profile is also measured.

3 Line profile asymmetries and deviations from gaussian shape

For most practical purposes, it is completely adequate to assume that an SWS instrumental profile is intrinsically a gaussian of FWHM corresponding to the resolution values discussed above. Small deviations from gaussian shape exist which in most real cases will be negligible, because low S/N and rebinning effects dominate the line profile. For certain high S/N observations, the question may arise whether observed deviations are real. Deviations from gaussian shape will also test any physical model of the SWS lineprofiles.

We have followed a dual approach of both deriving averaged line profiles for possible future analysis which are stored as a database, and parametrizations aiming at describing some of the most important properties of the line profile. The average line profiles are derived by rebinning the ‘dot cloud’ of a flatfielded SWS AAR, using a binsize of 1/5 of the line FWHM (see Section 6 for details). Our line profile parametrization follows an approach frequently used in astronomy (e.g. [Heckman et al. 1981]), which measures the line centroids and widths at various heights. In our case we use the rebinned average profile to measure these quantities at 80, 50, 20, 10, 5, 2, and 1% of the peak height of a gaussian fitted to the line dot cloud in the flatfielded AAR. To this we have added a line peak wavelength derived from a parabola fit to the dot cloud within 0.2*FWHM from the centroid obtained from the gaussian fit (to test claims of an offset between gaussian fit centroid and peak position derived in such a way), and the actual peak height of the average profile. Fig. 15 visualizes this for an example profile. For convenience, all quantities are normalized to the gaussfit FWHM, and the centroids refer to the center of the gaussfit.

Height(%)	Center	Width	Notes
100	0.0004±0.011		Peak height: 0.9926±0.0029
80	-0.0002±0.009	0.560±0.015	
50	-0.0007±0.008	1.002±0.011	
20	-0.0016±0.010	1.535±0.014	
10	0.0008±0.011	1.845±0.018	
5	-0.0002±0.009	2.103±0.016	
2	0.0017±0.010	2.401±0.025	
1	0.0030±0.007	2.603±0.020	

Table 3: Line profile parameters for a simulation using as input 31 ideal gaussian lines, with realistic SWS sampling at different wavelengths. Mean values and the standard deviation of individual measurements are given

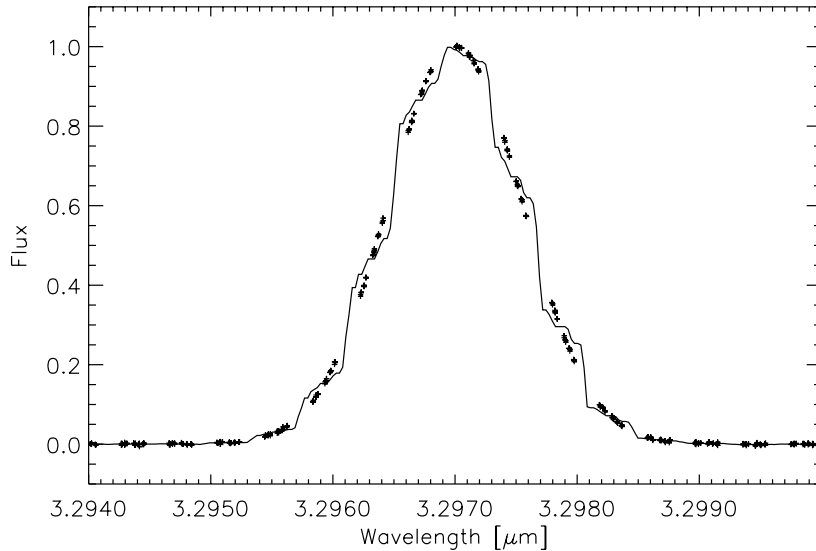


Figure 16: Rebinned line profile for a simulated perfect gaussian line near $3.3\mu\text{m}$. Details of SWS sampling introduce ‘stairs’. The original data points are shown by crosses.

3.1 Reference quantities for an intrinsically gaussian line

The derivation of an average line profile includes a rebinning step which will induce slight deviations from gaussian shape even if the intrinsic profile were perfect gaussian. When assessing non-gaussianity of the profile, comparison should be made not to widths computed for an ideal gaussian, but to widths obtained from a realistic simulation. For SWS, details of the average rebinned profile depend on the sampling which differs between different wavelengths. It is hence not sufficient to obtain a single such simulation. We have tried to obtain an overview by replacing all flux values of an otherwise unchanged SWS02 on NGC 7027 with a superposition of ideal gaussian lines with a very small noise (0.002 of peak) added. The simulated data were run through the CAP and the resulting 31 line profiles analysed in an identical way to the real data. Table 3 summarizes the resulting parameters.

A first conclusion from Table 3 is that already the sampling of a SWS02 line profile limits the accuracy of profile parameter determinations to about 1% for an individual measurement. A closer inspection of the 31 test lines revealed that for most wavelengths the accuracy in such an ideal simulated case may be slightly better, the overall standard deviation being pushed up by two lines in the $3.1\text{-}3.3\mu\text{m}$ range. For this range, the separation of detectors of the SWS array, expressed in steps of the grating scanner, is close to an integer, leading to almost identical sampling of the line by all twelve detectors. Unlike the typical case, where small offsets between the sampling provided by each detector lead to a dense overall sampling, such a coarse sampling leads to a ‘staircase’ shape of the rebinned profile (see e.g. Fig.16) which is obviously not suitable for the type of detailed profile analysis described here. This type of coarse sampling occurs for parts of SWS band 1 where the detector separation is very close to 3 scanner steps, namely near $2.5\mu\text{m}$ and near and above $3\mu\text{m}$. A less obvious coarse sampling also occurs in some regions of other bands where the detector spacing is close to a multiple of 0.5 scanner steps.

3.2 The SWS profiles

Figure 17 shows example profiles for all four bands, taken from the brightest available lines without disturbing intrinsic line structure. The salient points emerging from inspection of the line profiles above about 1% of the peak height are:

- All lines are close to gaussian
- A faint blue wing is observed in band 3
- For these strong lines, band 2 and more clearly band 4 show wide faint wings on both sides.

In a more systematic way, these features can be analysed using Figures 18 and 19 which plot the profile parameters (centroids, widths, peak height defined in Figure 15) as a function of wavelength for all measurements which were good enough to derive them. Above about 20% of the peak height, the measured center and width parameters are identical to those expected for gaussians, within the small scatter. This is also true for the peak height since the larger values measured for some noisy lines (small symbols) can be due to simple noise, and since the peak value is defined as the simple maximum of the rebinned profile, i.e. sensitive to noise and biased towards higher values in the presence of noise.

For band 3, the faint blue wing is reflected in significantly negative centroid values at 1-2% height, reaching ~ 0.1 of the FWHM. The accompanying width increase is modest, suggesting that most of change is indeed in the blue wing. Variations of the blue wing seen with location of the source within the SWS aperture (Figure 27 below) suggest this wing to be an optical effect. A less pronounced blue wing at 2-5% height is suggested, with poorer significance, for the brightest lines in band 2 (e.g. [S IV] $10.51\mu\text{m}$). For bands 1 and 4, the presence of such wings can neither be confirmed nor rejected. In band 1, blue He I satellites/wings to all the bright recombination lines prevent line profile analysis to the required depth. Similarly, in band 4 S/N does not allow to probe the 1% level well. Data at higher level perhaps suggest that no blue wing is present in band 4 (Fig. 18).

The faint and more symmetric wings seen for the band 2 and 4 lines in Figure 17 are, for the case of band 2, reflected in large line widths measured at low heights (Figure 18). Again, the automatic routine does not probe deep enough for band 4 to quantify this behaviour, but wings as in Figure 17 are evident in band 4 scans of bright lines. While the wings are seen in SWS02 scans, they may be somewhat cut there because of the limited scan range. For band 4, perhaps the entire wings can be

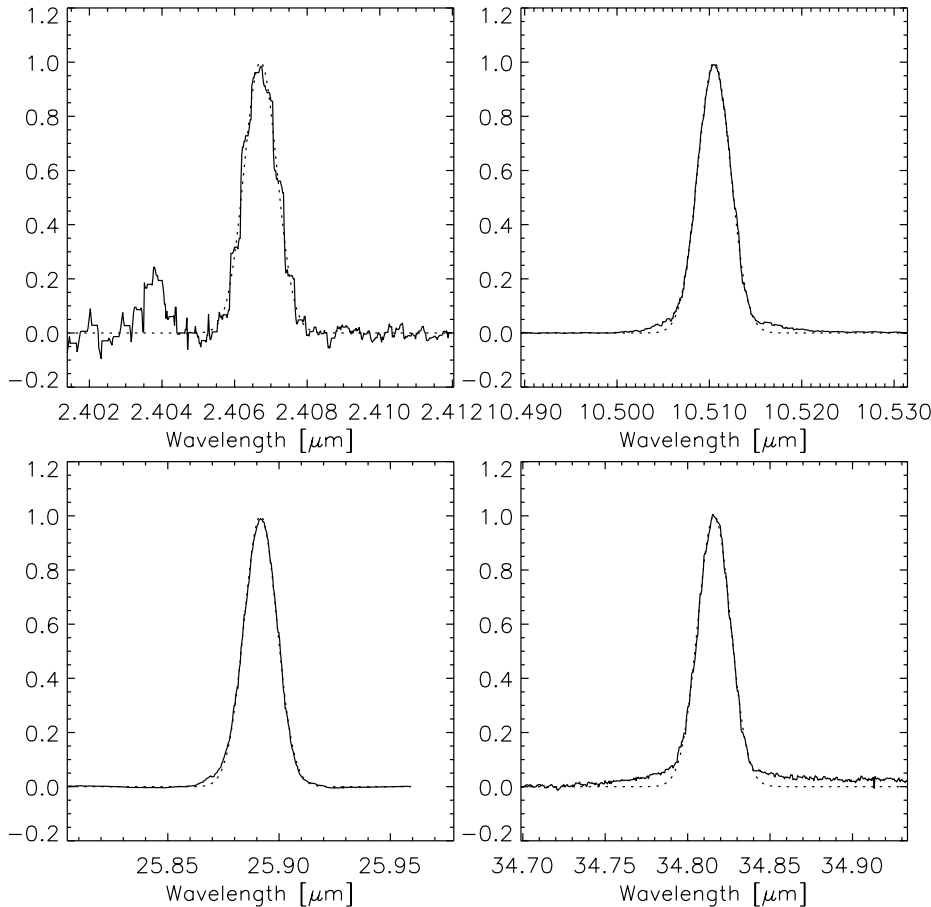


Figure 17: Some examples of SWS line profiles from bands 1 to 4. For band 1, the brightest lines are recombination lines with real He satellites causing blue wings (Figure 23). The line shown is hence a fainter H₂ line, falling also into a range of nonideal sampling (see Figure 16). All profiles are close to the gaussian profiles which are shown dotted for comparison. The most noticeable deviations are blue wings in band 3 (see also Figures 15 and 27), and faint (percent level) wings seen near very strong lines in band 2 and most clearly band 4.

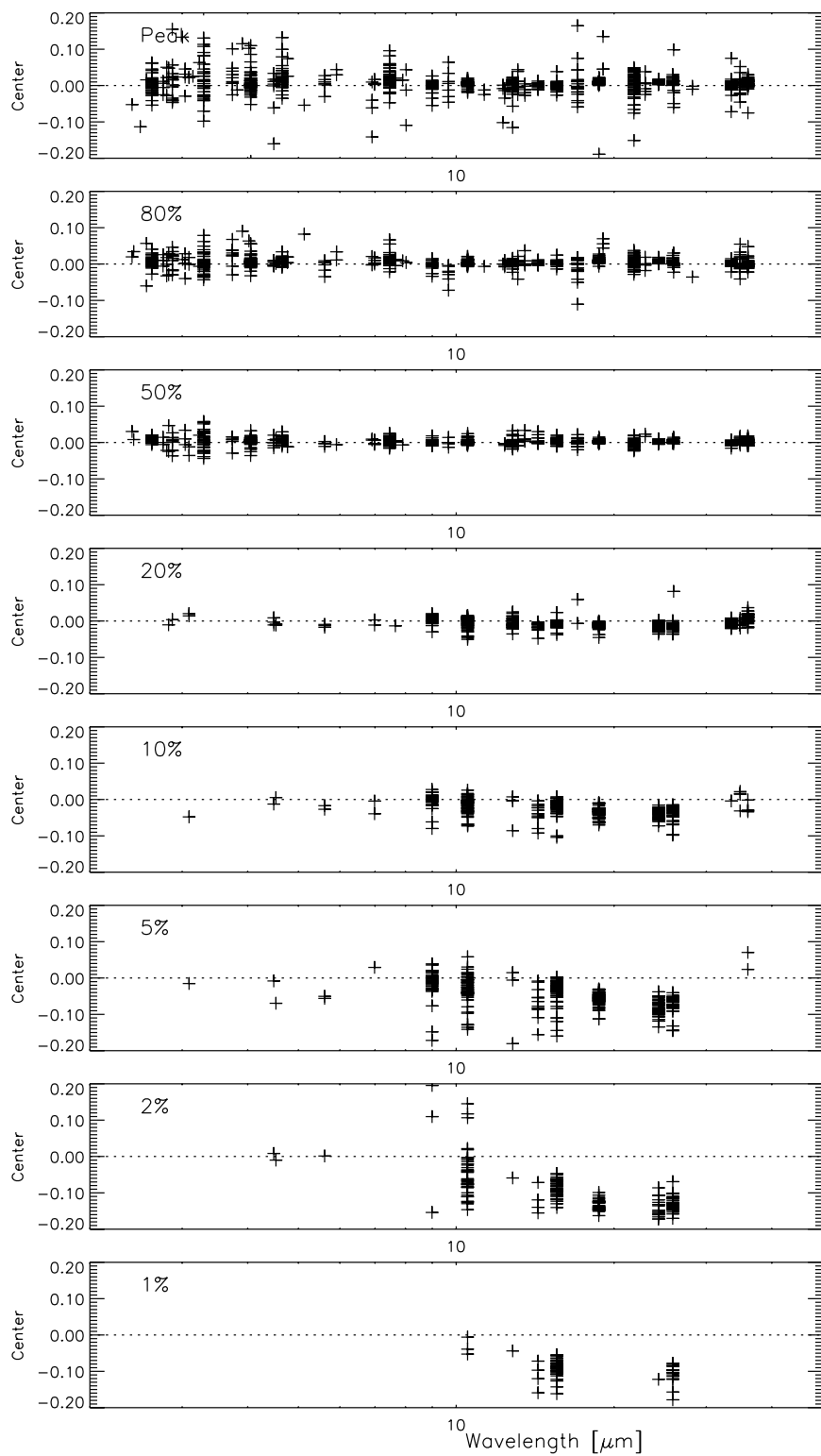


Figure 18: Shift of line centroids at various heights relative to the gaussfit centroid. The shift is normalized to the gaussfit FWHM.

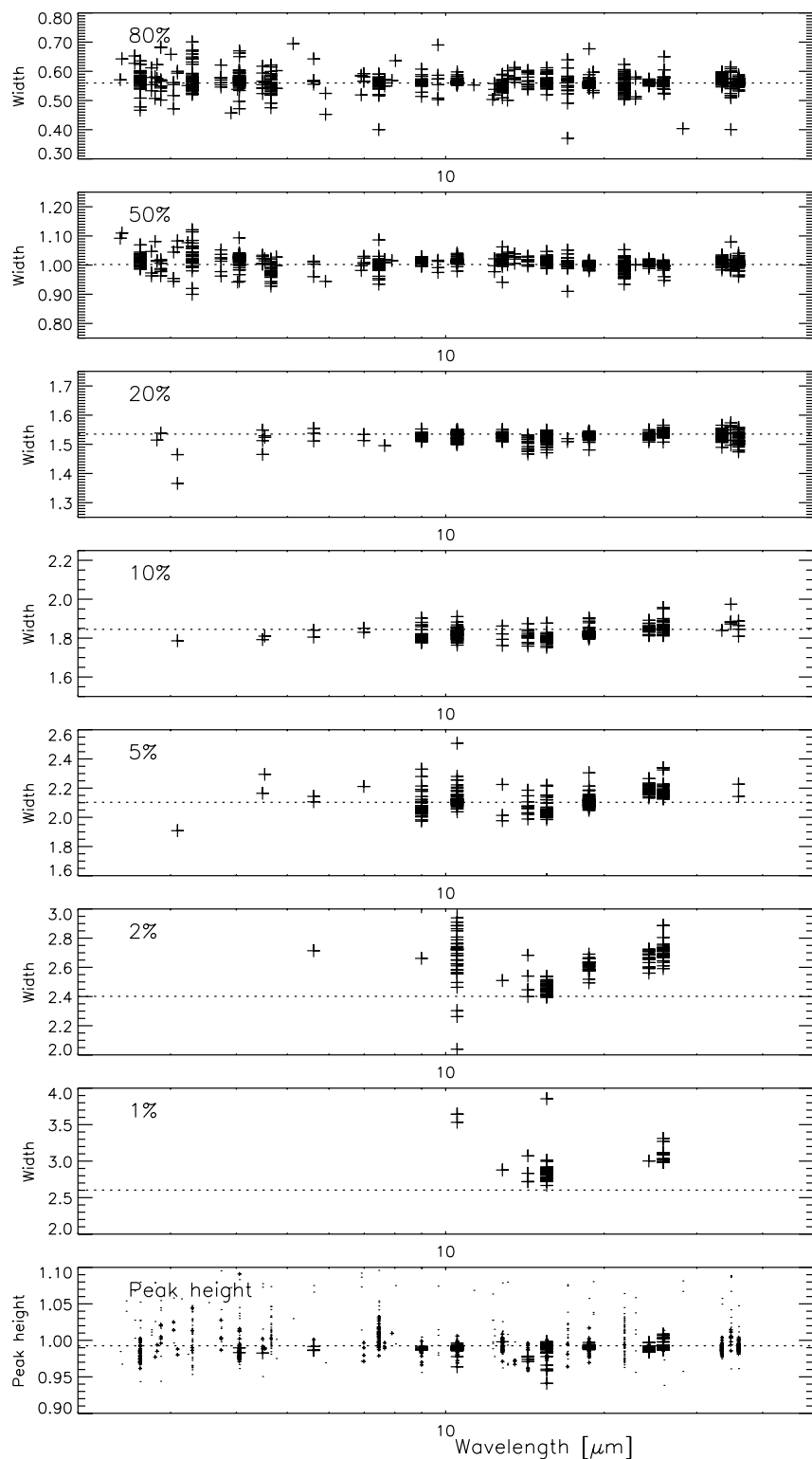


Figure 19: Line widths at various heights, normalized to the gaussfit FWHM. The dashed lines indicate expectations for a purely gaussian profile subjected to the same rebinning. The lowest panel shows peak heights of the rebinned line profiles, normalized to the peak height of a gaussian fitted to the raw dot cloud. The dashed line indicates the expectation for a purely gaussian profile subjected to the same rebinning.

due to the effect of detector transients (see section 5). For band 2, this situation is less clear. Most likely, we see a mixture of an optical effect, analogous to the band 3 wing but more symmetric, and detector transients (see sections 3.3 and 5). Transients are known to be present in bands 2 and 4 but almost absent in bands 1 and 3.

The proposed origins of the band 3 (and others?) blue wings – optical effects – and the band 2,4 faint wings – detector transients – might also be tested by looking for trends with line flux which should exist for the second but not for the first. Unfortunately, the wings can only be quantified for very bright lines, leaving too little dynamic range for any meaningful analysis of trends with flux.

3.3 Probing the mud: Line profiles below 1% of the peak height

For some of the brightest lines, the plain signal-to-noise ratio is sufficient to probe structure in the line profiles to below the percent level. We present some tentative results and interpretation, but warn that they are uncertain for various reasons:

- Systematic effects in data analysis become important. In particular, the SWS02 scans do not provide sufficient wavelength coverage to reliable cover faint wings. In addition, flatfielding of the partially overlapping ranges produced by the twelve detectors will introduce systematics that will depend on details of the reduction recipe. Fringing will become noticeable even for sources with reasonably faint continuum.
- There are only very few sources of sufficient brightness in general, and not all of them have been observed in a suitable mode. This causes difficulties to distinguish instrumental properties from putative faint high velocity components, and to look for trends with flux.

Figures 20 and 21 show some examples of SWS02 line profiles at these faint levels. Note again that various systematics may influence them at the lowest level. The faint wings on both sides of band 2 lines are clearly seen. Apparently, for lines like [SIV] the blue wing is stronger at the 2-5% level but the red wing stronger below 2%. This may be reflected in the line centroid being on average more blueshifted at the 2% level than at the 1% level for the [SIV] line (Figure 18). In band 2, there is considerable variation from source to source. The stability of band 3 profiles suggests this to be *not* scatter in source properties but more related to line flux. The lines in the lower right panel of Figure 20 are fainter than those in the lower left panel. Overall, these wings most likely are a mixture of optical effects (as in band 3 but more symmetric), and detector transient effects as in band 4 (see Section 5).

The Band 3 lines are nicely reproducible from source to source, and the blue wing is clearly seen. The $\sim 0.2\%$ U-shape of the continuum is likely due to the flatfielding procedure with a possible contribution of other effects (in particular fringes).

At the very faintest level, wings of $\sim 0.2\%$ of the peak are seen in some long SWS06 scans of band 2C lines, extending to $>1000\text{km/s}$ (>8 FWHM) from the line center (Figure 22). SWS06 scans are much more reliable than short SWS02 scans for probing this kind of structure. In one line, these wings have been observed in two sources and are very similar, suggesting an instrumental origin. They are very similar in up- and downscan, suggesting an optical origin rather than detector transients. Such wings cannot be detected reliably in the SWS02 scans - the SWS02 data for the same sources are, however, consistent with what is seen in SWS06.

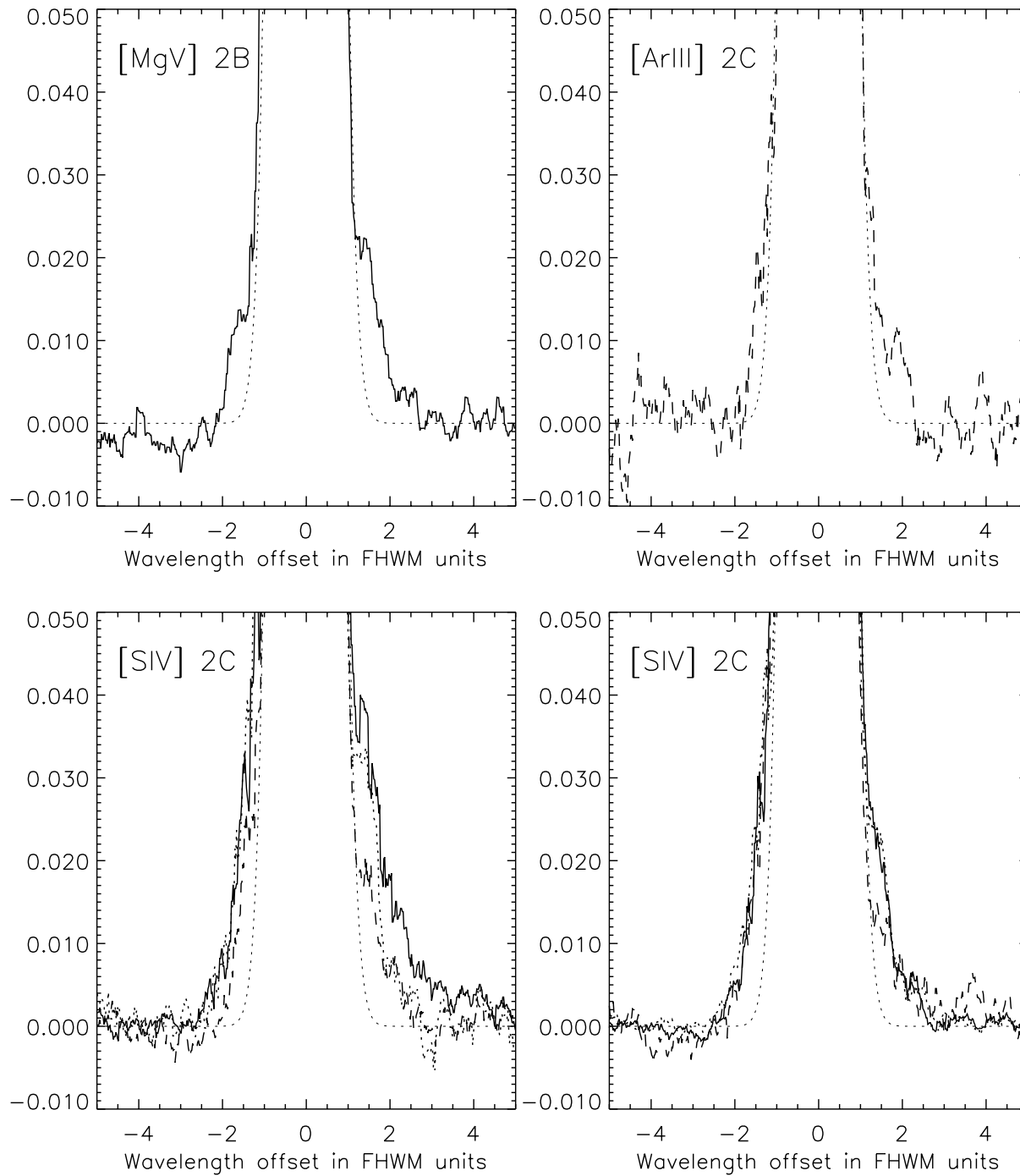


Figure 20: Some examples of line profiles at very low level (<5% of the line peak). Different line styles code different sources, codes may differ from panel to panel. The gaussian best fitting the entire profile is overplotted. Note that the profiles have been derived from SWS02 scans of limited width and are clearly suffering from systematic problems at the lowest levels!

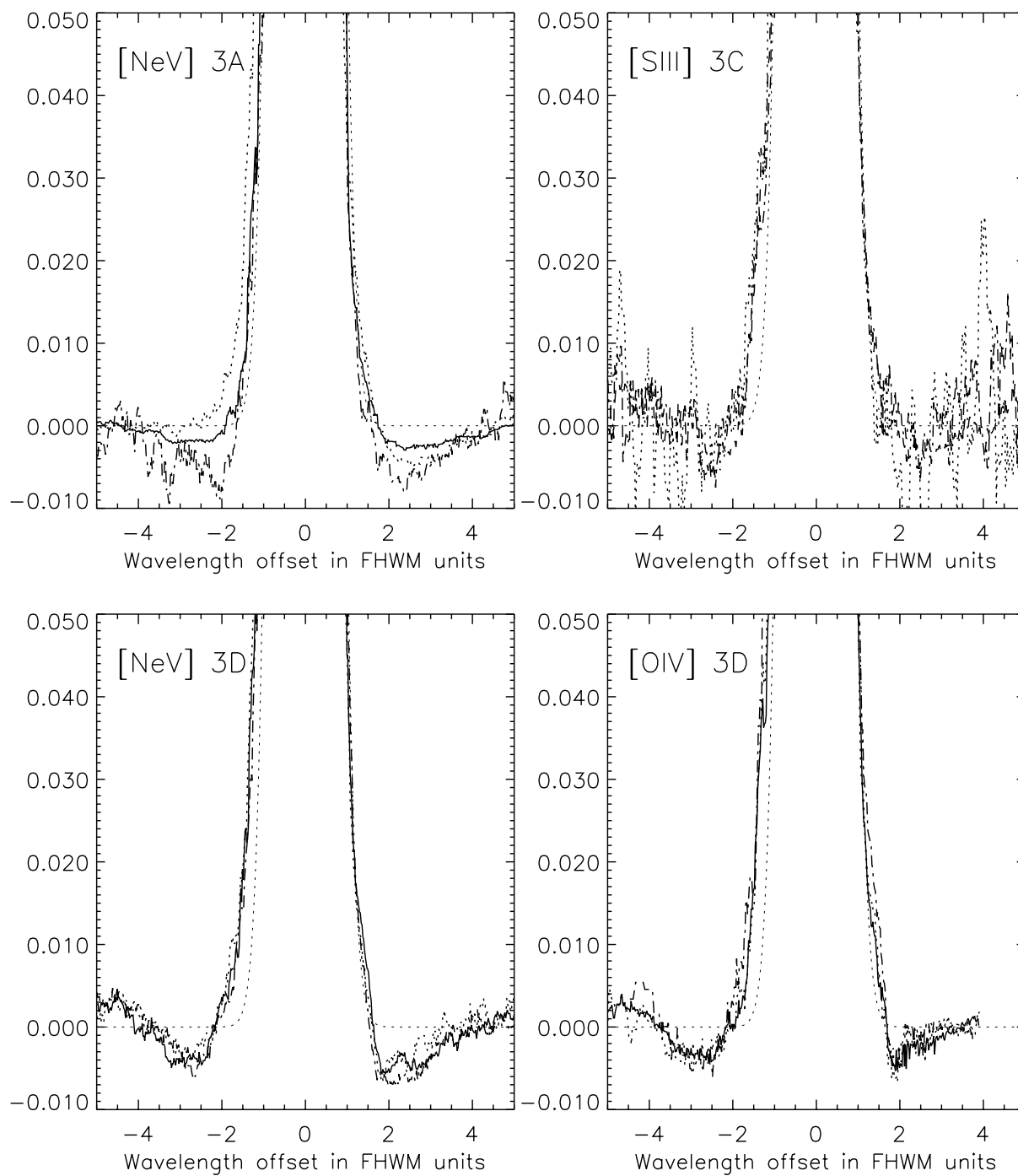


Figure 21: Examples of line profiles at very low level, as in Figure 20

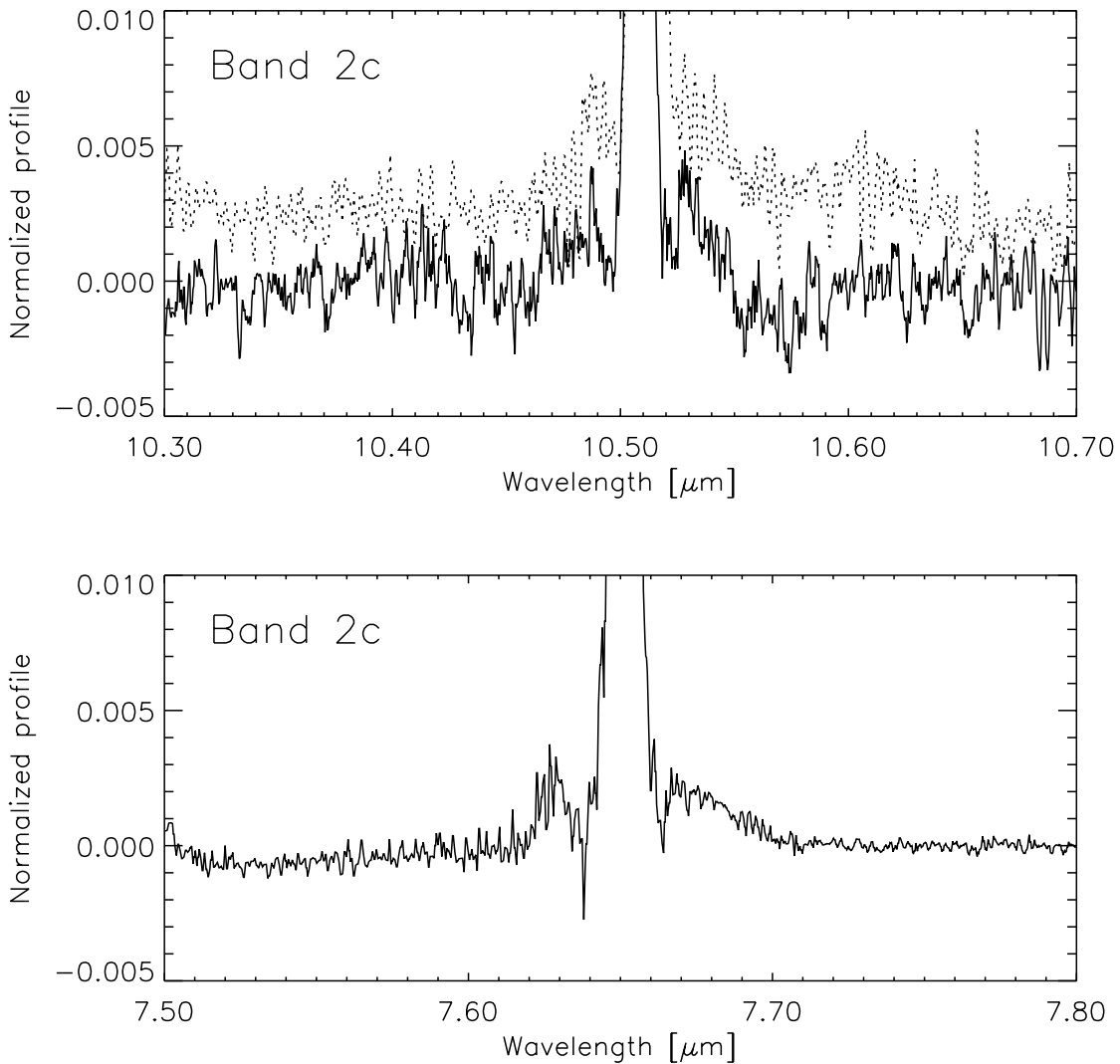


Figure 22: Some examples of line profiles at very low level (<1% of the line peak). The profiles are taken from SWS06 scans covering a large wavelength range. In the top panel, two independent planetary nebulae are shown offset, showing similar wide wings at the 0.2% level. This suggests an instrumental origin rather than an intrinsic high velocity component of the sources.

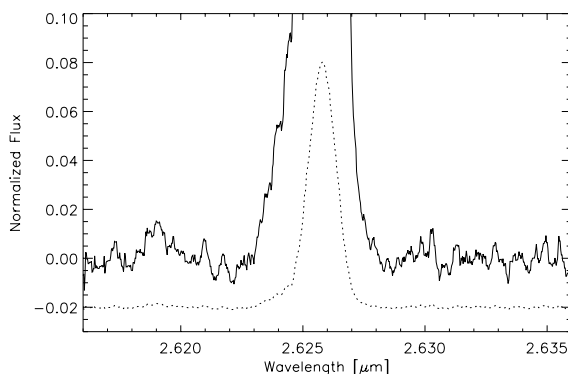


Figure 23: Satellites seen close to bright hydrogen recombination lines (here Brackett β) are due to HeI recombination, i.e. not instrumental ghosts. This is also the case for the blue wings of these lines.

3.4 Search for ghosts

During analysis of the SWS profiles we have also searched for possible ghosts, i.e. unidentified well-defined lines close to bright lines which might have an instrumental reason rather than being real. No such lines have been found, down to a level which reaches 1% of the nearby bright line in favourable cases. Note that in SWS02 scans, satellites are seen close to bright hydrogen recombination lines, these are however real, being due to HeI just like the blue shoulders to the H lines. Such satellites have seen close to Brackett β (see Fig. 23) and Brackett α . In wavelength and flux, they match well the expectations from HeI recombination theory ([Smits 1996], [Smits 1998], see also [Rubin et al. 1998]).

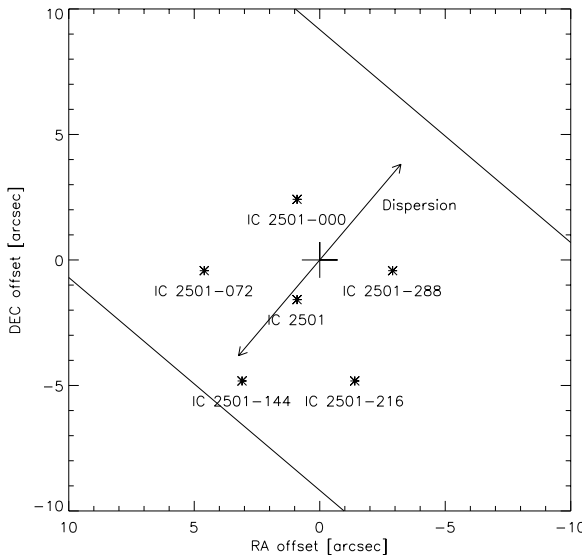


Figure 24: Positions of the pentagon of offset observations around IC 2501, relative to the cross marking the nominal position of IC 2501. Asterisks denote the reconstructed actual pointings (taken from OLP version 6.32). At this early stage of the mission, a significant pointing error was present. Arrows indicate the dispersion direction, the two lines orientation and width ($14''$) of the slit for bands 1-3 centered on the nominal position.

4 The effects of mispointing: A test

Slight pointing errors affect SWS observations in several ways, the most obvious being flux loss when leaving the tip of the beam profile, and shifts in observed wavelengths. To specifically address the second topic and related effects on the instrumental profile, dedicated observations have been executed in Revolution 44 which consist of a standard SWS02 observation of the compact planetary nebula IC 2501 in several bright emission lines, plus identical off-source observations forming a pentagon of 4 arcsecond radius around the nebula (Fig. 24). E.Valentijn in [SWS PV report 1996] and [van den Ancker et al. 1997] give a preliminary summary of these observations. IC 2501 being a southern source, there are no published high resolution radio observations to constrain its diameter, quoted optical diameters vary somewhat, we have adopted $<2''$ (ApJS 14,154). The intrinsic line width is not published, we have adopted 35 km/s, a reasonable value for planetary nebulae. Figure 25 summarizes the mispointing effect on the emission lines: There are both shifts and shape changes of the lineprofiles. The observed pattern of wavelength shifts and flux changes is consistent with the reconstructed pointing shown in Fig. 24. Due to a slight pointing error as typical for the early ISO mission, the pentagon is not centered on the source. We have also taken the opportunity to revisit the issue of resolution for point- and extended sources by producing a simulated $\sim 8''$ diameter source out of the coaddition of all 5 pentagon spectra and the central spectrum, and analysing it in the same way.

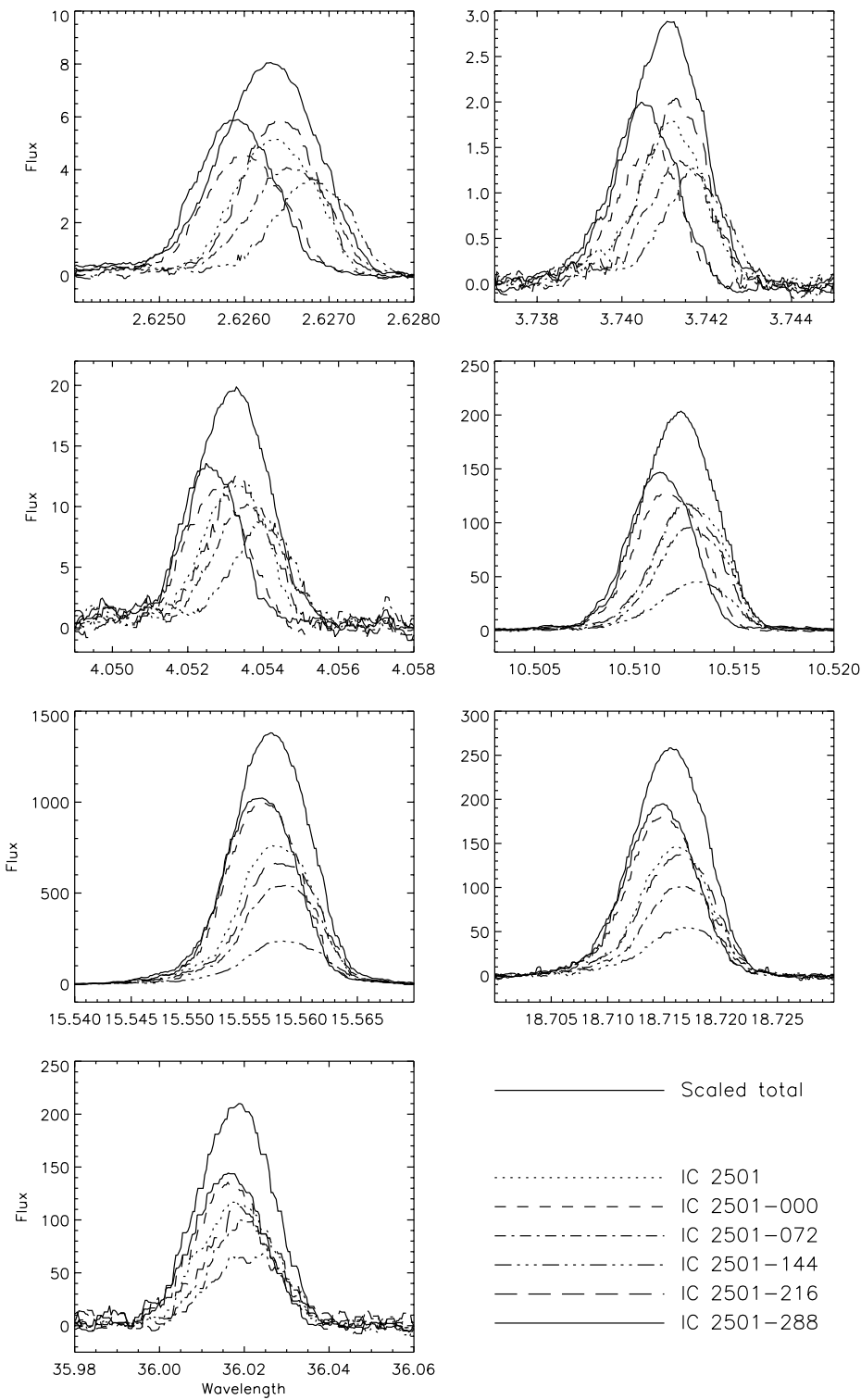


Figure 25: Lineprofiles of seven bright emission lines for IC 2501, for a pentagon of offset positions encircling IC 2501, and for a total spectrum simulating a somewhat extended source. Note that the total spectrum is scaled for plot reasons.

4.1 Wavelength shifts

The obvious wavelength shifts caused by the large pointing offsets between the pentagon positions can be used to get some kind of worst-case estimate for the impact of pointing uncertainties on the SWS wavelength calibration. To derive such a quantity, we have expressed for each line half the shift between the two most extremely shifted lines in km/s. This corresponds to a shift in dispersion direction of $\sim 3.5''$ which may be a reasonable value for a pointing uncertainty in the early phases of the mission (REV < 360) when the pointing was more uncertain than later. The result is summarized in Table 4. Very large mispointings due to observer error could cause shifts higher by another factor ~ 2 .

Line	λ	Velocity uncertainty
Br β	2.62	52km/s
H 8-5	3.74	48km/s
Br α	4.05	51km/s
[S IV]	10.51	24km/s
[Ne III]	15.55	20km/s
[S III]	18.71	16km/s
[S III]	36.01	20km/s

Table 4: An indicator of the uncertainties of SWS-measured radial velocities that might occur in case of strong ($\sim 3.5''$) pointing errors, derived from the IC2501 ‘pentagon’. Note that both higher and lower values will be found at other SWS wavelengths.

The highest pointing-induced wavelength shifts are found in the SW section where the ISO diffraction disk is small compared to the SWS aperture. In that section, the largest shifts in terms of km/s may be expected in those regions of the 2.4-12 μ m range where the resolution is lowest, for example near 3.5-4 and especially 5.3-7 μ m.

4.2 Resolution

Analogous to the decrease of resolution that is found when going from a point source to an extended source, an increase in resolution would be expected for a point source just at the edge of slit, since the profile entering SWS is even narrower with half the diffraction disk cut away. Table 5 summarizes the measured resolutions for the various positions, with the first row representing the observation aiming at the nominal source position of IC 2501 (but slightly offset, see Fig. 24), the second last row the simulated extended source, and the last row an average of results for three positions close to the slit center (see below).

There is no evidence for an increase of resolution at edge positions. Comparing an average resolution for positions IC2501, IC2501-000 and IC 2501-288 which are all close to the slit center with IC2501-144 which is closest to the edge, the resolution for the ‘edge’ position is *lower* than for the center, not higher as expected on the basis of slit input with a cut diffraction disk. The trend towards lower, not higher resolution at the slit edges is also seen in Figure 26 which shows the measured resolution as function of the line flux which is lowest at the edge of the slit. This unexpected finding reflects most likely a not well understood behaviour related to the blue line wings which are visible more strongly in the edge position (see Fig. 27). The simulated extended source clearly produces 10-20% lower resolution at the shortest wavelengths. At wavelengths of 15 μ m and longer, the resolution decrease is

Source	2.62	3.74	4.05	10.51	15.55	18.71	36.01
	H6-4	H8-5	H5-4	[S IV]	[Ne III]	[S III]	[Ne III]
IC 2501	2437	2044	2078	2645	2076	2698	1812
IC 2501-000	2342	2142	2116	2717	2138	2615	1844
IC 2501-072	2382	2032	1877	2612	2058	2542	1902
IC 2501-144	2535	2130	2112	2586	1948	2217	1765
IC 2501-216	2595	2214	2101	2763	2048	2545	1827
IC 2501-288	2458	2069	2230	2852	2152	2673	1873
IC 2501 'Total'	1995	1816	1825	2504	2014	2496	1795
Slit center	2412	2085	2141	2738	2122	2662	1843

Table 5: SWS resolution (not corrected for intrinsic linewidth) of the seven bright lines observed at the various IC 2501 pentagon positions and the simulated extended source. The last row is the average of three positions close to the slit center.

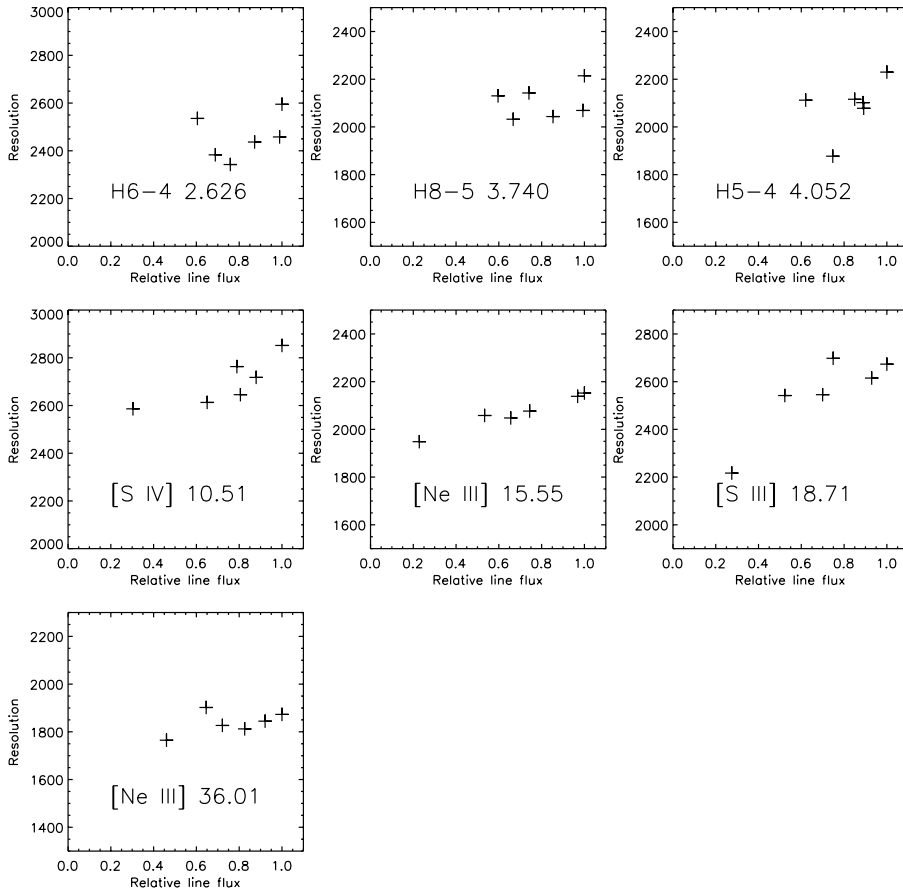


Figure 26: Resolution measured for the IC 2501 pentagon observations as a function of line flux which has been normalized for each line to the brightest flux in the pentagon. The trend towards low resolution at low flux contradicts the expectation that positions close to the slit edge should show both low flux and enhanced resolution.

at most a few percent for this simulated source of about 8 arcseconds diameter.

4.3 Profile shapes

Figure 27 shows a representation of the IC 2501 lineprofiles which is more suitable to find small line profile variations than the direct visualization of Figure 25. Within the signal-to-noise of the data, the profiles are surprisingly constant with the exception of a variation in the blue wing of the line profile which is visible in all three high S/N profiles ([S IV], [Ne III], and [S III]). This variation is most pronounced in position IC2501-144 which is closest to the slit edge. The reason for this wing must hence be dependent on the slit illumination, suggesting an origin early in the SWS optical path before the dispersing grating.

For reasons of low signal-to-noise in the other lines, and blue satellites to the hydrogen recombination lines, we have quantitatively analysed profiles only for the [S IV], [Ne III], and [S III] lines. Figures 28 and 29 show the results expressed in terms of the line centroids and widths defined in section 3. Some variations at faint level appear to be significant and reflect the mentioned variations of the blue wing, it should however be noted that such modest variations will be visible only in high S/N data. For the Br β profile, we see no evidence for the ‘ghost’ at $2.6288\mu\text{m}$ reported in [SWS PV report 1996], down to a level of 2% of the line peak.

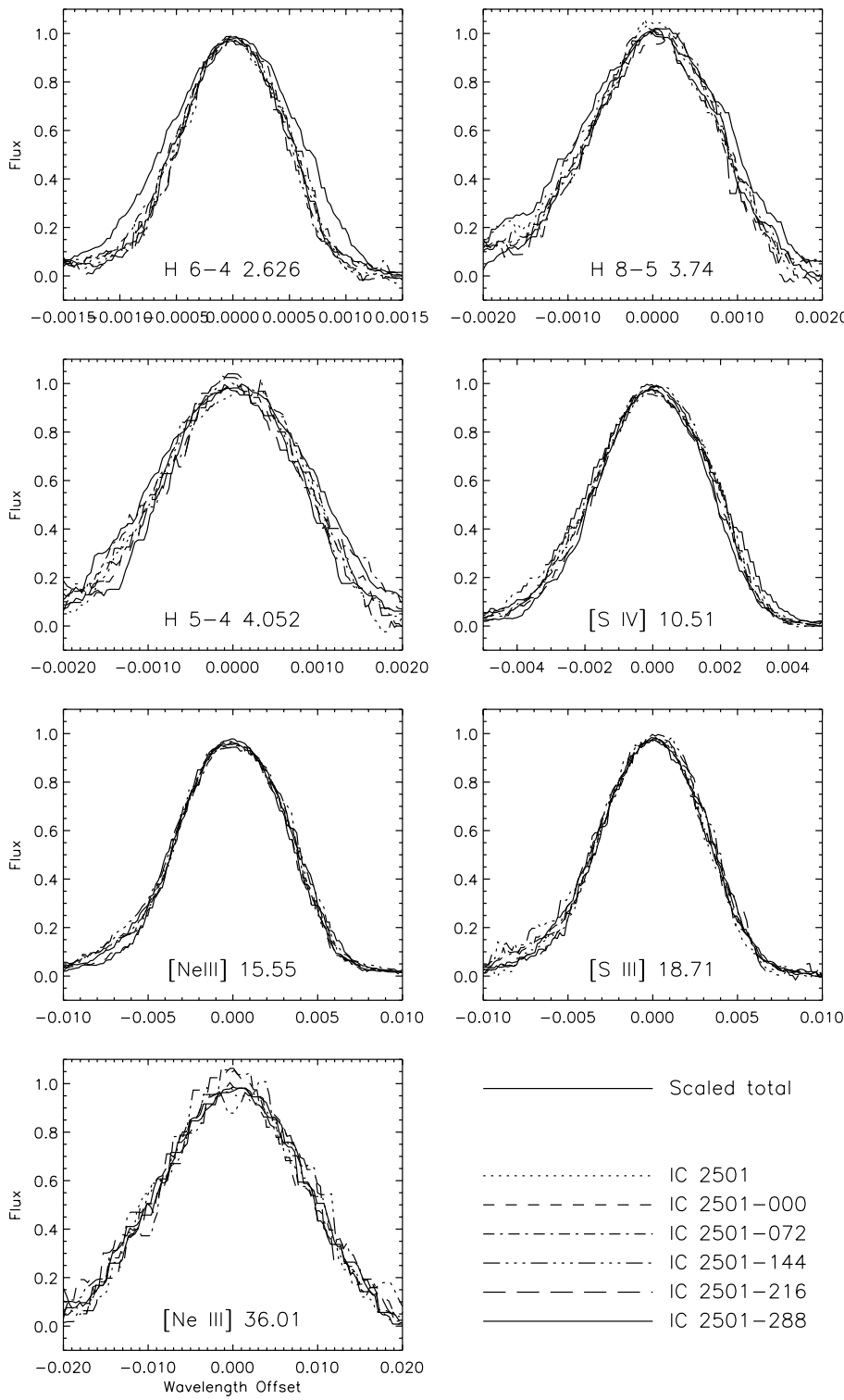


Figure 27: Lineprofiles for various positions of the pentagon and simulated total, as already shown in Figure 25. To highlight possible profile shape variations, the profiles have been normalized in flux and shifted to same central wavelength.

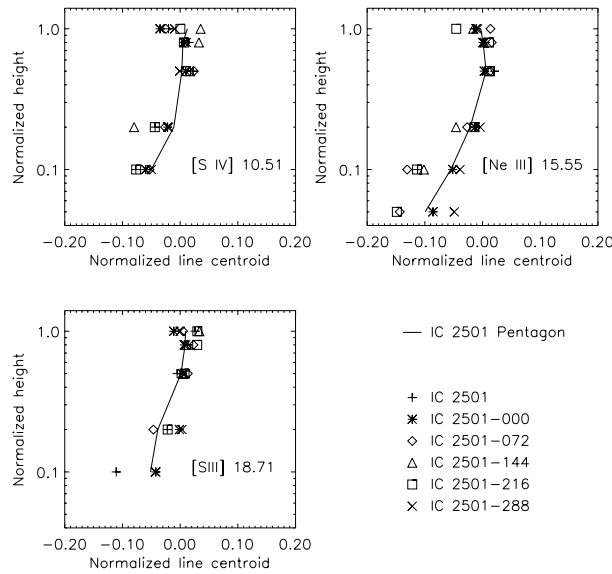


Figure 28: Line centroids at various heights for the observations of the IC 2501 pentagon. Centroids refer to the gaussian fit center and are normalized to the gaussfit FWHM.

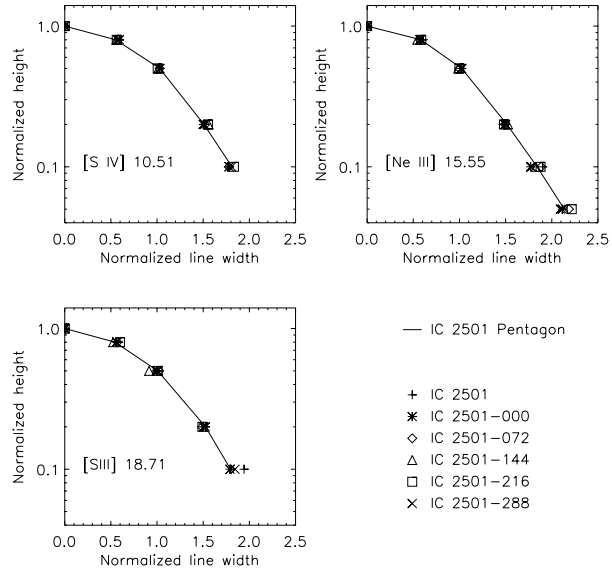


Figure 29: Line widths at various heights for the observations of the IC 2501 pentagon. Widths are normalized to the gaussfit FWHM.

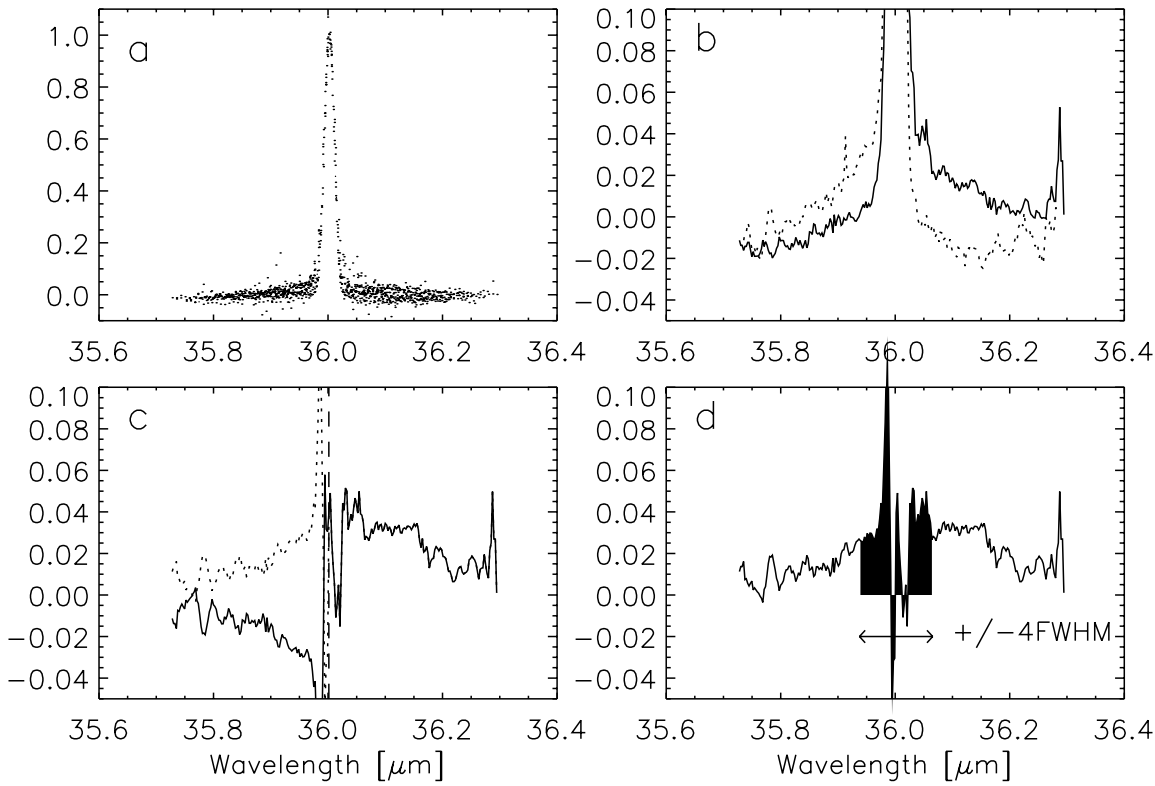


Figure 30: Effects of detector transients on line profiles, and their parametrization. (a) AAR dot cloud for a strong [Ne III] $36\mu\text{m}$ line. There is already an indication for faint wide wings. (b) Upscan (dotted) and downscan (continuous) have been averaged separately to show the typical pattern of steep rise but slow decay. (c) The difference of down- and upscan (continuous) shows a typical S-shape residue which would be absent in the absence of memory effects. The part of the residue shortwards of the line center is inverted (dotted) to produce a transient signature which is overall positive. (d) The residue is averaged, in this example over a total range of 8 times the line FWHM indicated by the black area. Note that the method is also sensitive to steady underlying drifts not related to the line, but in a way that will return the largest signal over large rather than small ranges.

5 Detector transients: Effects on Line profile

The response of photoconductors like those used in SWS to changes in the incident radiation is not instantaneous. ‘Transients’ or ‘memory effects’ are observed in the step response which can happen on timescales up to many minutes which depend on detector material, flux level, and flux history. In principle, these effects may also distort the observed line profiles, leading to an asymmetry between rising and falling slope of the line. Since all SWS02 scans are done first up in scanner positions (corresponding to down in wavelength) and then back down, comparison between up- and downscan can probe for the presence of such effects and provide parametrizations. The treatment we have chosen is explained in the caption of Figure 30.

Transients usually take the form of a very fast initial response to a flux change, followed by a much slower drift towards the final stabilized signal. Under conditions typical for SWS operation, the time

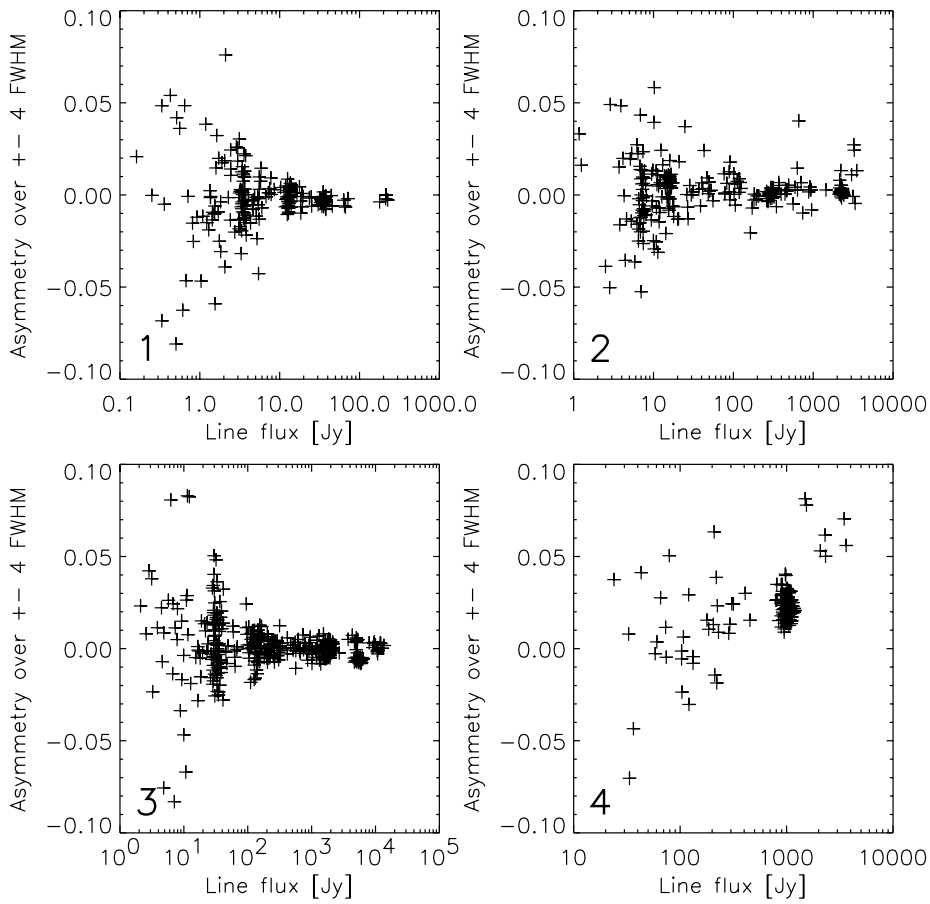


Figure 31: Asymmetry of up- and down scan averaged over ± 4 FWHM, as a function of line flux. The four SWS bands are shown separately.

constant of these drifts will be slower than the few seconds used to scan across the line. Then, transients should express themselves in uncertainty of the total line flux and slower drifts outside the line rather than distortion of the shape of the inner part of the line. Our comparison between up- and downscan does not probe well for possible transient effects within the inner part of the line. Here, transient effects are difficult to discriminate from others: Small shifts can occur due to grating scanner hysteresis or ISO pointing jitter, and pointing jitter can also introduce flux changes. Independent empirical confirmation that transients should not be important for the shape of the inner part comes, however, from the fact that resolution apparently does not depend on line flux (Figs. 9,10).

Figures 31 and 32 show that there is no indication for transient effects on line profiles in bands 1 and 3. The scatter in asymmetry measured at high line fluxes is in fact remarkably small, indicating low grating scanner hysteresis and good pointing stability. Very clear transient effects are seen in band 4. This and presentations like in Figure 30b suggest that most of the faint wings seen in band 4 detectors are induced by detector transients. The situation is less clear for band 2. Some indications for transient effects are seen, more clearly in the correlation with continuum flux than with line flux.

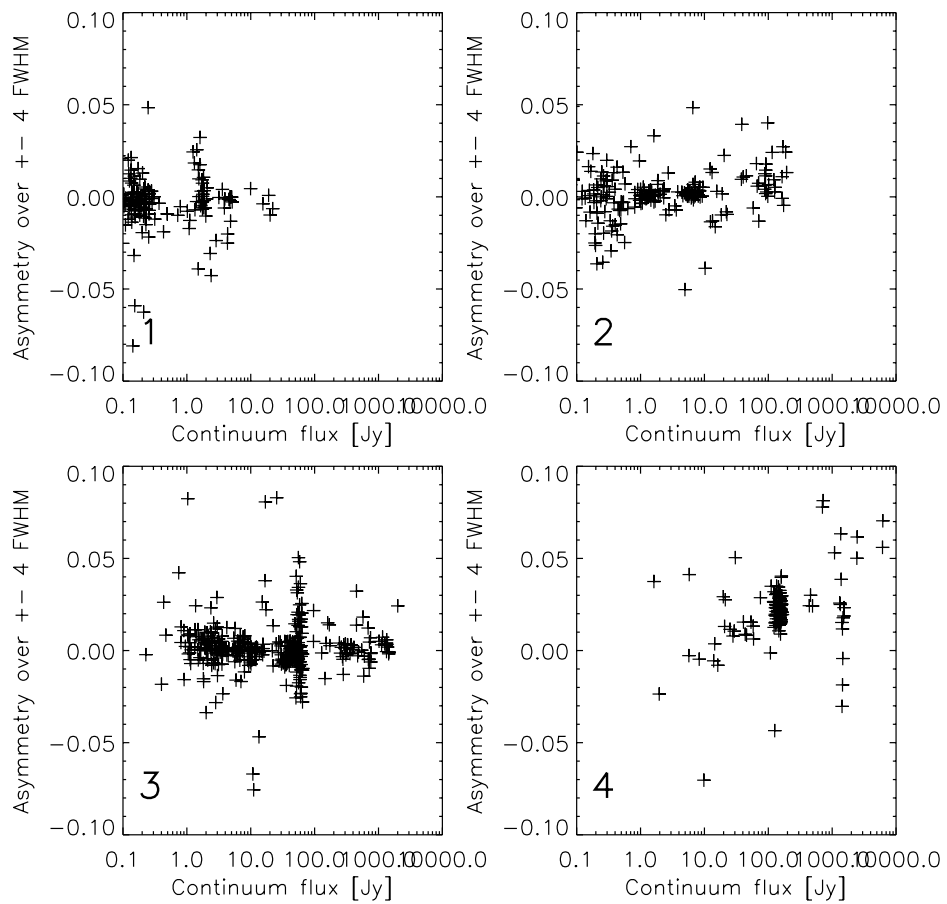


Figure 32: Asymmetry of up- and down scan averaged over ± 4 FWHM, as a function of continuum flux. The four SWS bands are shown separately.

Given that the wings are less pronounced in band 2 (Figure 17), transients may still be the main responsible.

6 Appendix: Description of CAP 6.3.2.1

SWS data reduction recipes are not fully standardized and inevitably include steps of clipping outliers and of rebinning the AAR dot clouds into single-valued spectra. These steps may affect the derived line profiles. Different users may use different code and parameters, also guided by their knowledge of source properties like intrinsic line width. Hence, ‘the’ line profile is only a somewhat uncertain concept. A user who wants to compare his results to standard values must be aware of the steps taken in deriving them, for example to be sure whether a larger linewidth is a real source property or perhaps just a consequence of different rebinning parameters. For reference, this section summarizes the most salient features of the CAP used for line profile determinations.

The basic approach was to use largely automatic procedures, in order to be able to cover a large set of observations within reasonable time. This has a number of immediate consequences. The AAR product is used as starting point and should be produced by a recent pipeline version (7 or higher). No attempt of defringing the data is made. Interactive defringing of all data is prohibitive, and all current automatic defringing tools face difficulties with the special type of SWS02 data used here - experiments using **FRINGES** and **RESP_INTER** caused deterioration of data in test cases. This implies, in particular for band 3, that line profiles from low line-to-continuum data are more disturbed by fringes than a most carefully reduced and defringed science data set may be.

The basic flow of CAP 6.3.2.1 starts with an initial interactive inspection of each dataset, in order to identify lines suitable for profile fitting. Together with source-related parameters (size, intrinsic velocity width, heliocentric radial velocity), identifications of ‘useful’ lines are stored in a simple observation-specific ASCII file of strict format. Since all lines are not perfect in the sense of being isolated on nice continuum, it is possible to limit fits to a certain range, and to prevent analysis of faint wings of the profile which may be useless in case of line like hydrogen recombination lines which have helium satellites.

The routine **C321_LINES** is the key step doing the actual profile analysis and is described in more detail below. Several smaller routines, not described in detail here, assemble the results into larger datasets and analyse them for the parameters of interest. The structure format used for the large datasets (‘result structure’) is:

```
linestr={c321_res,$
    tdt      : ' '           ,,$ ; TDT number
    instra   : 0.D            ,,$ ; source RA (J2000)
    instdec  : 0.D            ,,$ ; source DEC (J2000)
    instroll : 0.D            ,,$ ; ISO roll angle
    aotn     : ' '           ,,$ ; AOT number
    source   : ' '           ,,$ ; source ID (unique string)
    size     : 0.              ,,$ ; diameter in arcsec
    sizeref  : ' '           ,,$ ; reference for size
    vwidth   : 0.              ,,$ ; velocity width in km/s
    vwidthref: ' '           ,,$ ; reference for vwidth
    vhel     : 0.              ,,$ ; heliocentric velocity in km/s
    vhelref  : ' '           ,,$ ; reference for vhel
    ident    : ' '           ,,$ ; line identification (unique string)
    line     : 0               ,,$ ; line tag from aar
    aotband  : ' '           ,,$ ; aotband id (string)
    fcont    : 0.              ,,$ ; continuum flux [Jy]
    fline    : 0.              ,,$ ; line flux [Jy]
```

```

noise      : 0.          ,$ ; noise indicator [Jy]
wcen       : 0.          ,$ ; observed wavelength [micrometer]
fwhm       : 0.          ,$ ; fwhm of total gaussfit [micrometer]
efwhm      : 0.          ,$ ; error of fwhm
detfwhm   : fltarr(12)  ,$ ; fwhm of gaussfits for 12 dets
peak       : 0.          ,$ ; actual peak height
center     : fltarr(8)   ,$ ; centers at different height
width      : fltarr(8)   ,$ ; widths at different height
asym       : fltarr(10)  } ; memory asymmetry parameter at 1-10 FWHM

```

6.1 C321_LINES.PRO

This routine derives lineprofiles and their parameters for a single SWS02 AAR and stores them in a result structure. The main steps are

- The AAR is cleaned from glitched, ool and masked points and **SIGCLIPPed** with sigma=3 to eliminate remaining outliers
- A single line is extracted from the AAR by means of the line tag and an optional range criterion.
- The line position is identified by doing a crude rebin and searching for the maximum of the rebinned data. Data for which this is not possible due to weak lines or severe flatfielding problems are not suitable for CAP 6.3.2.1.
- A first flatfielding is done by offsetting the median of points outside the line to the same value for all detectors. This is obviously not good for weak lines on a strong continuum with a steep slope, but ways to circumvent this (e.g. the flat_inter algorithm) were not considered here because we were aiming for simplicity and transparency of the algorithm.
- Line location and flatfielding are repeated since faint lines may be properly located only after the first flatfielding.
- The profile is normalized by fitting a gaussian plus continuum to the dot cloud, then subtracting the continuum and normalizing the gaussian. Because some SWS lines have wider than gaussian wings, a simultaneous line+gauss fit tends to put some of the line wings into the continuum. We reduce this effect by first fitting a straight line only to the continuum outside $\pm 3 \times \text{FWHM}$ from the line center, subtract this linear continuum, and then fit a gauss only to the already continuum-subtracted profile. Such a compromise is required by the limited SWS02 range but is still not perfect for very wide wings like sometimes observed in band 4.
- If the data for a single detector meet a certain minimum line S/N and include the line, normalization is improved by a dedicated fit of a gaussian to the data for that detector, and normalizing by its peak value. The FWHM values for all such detectors are stored individually.
- The FWHM of the line and corresponding resolution are defined by fitting a gaussian *to the normalized total dot cloud*, i.e. to the data without any rebinning!
- A rebinned version of the line profile is produced using the aarfilt routine and a binsize of 1/5 of the FWHM. This is a smaller binsize than likely used for most science data reductions, and causes only small distortions of the ideal profile.

- A noise indicator is determined as the standard deviation of the rebinned spectrum far off the line. Note, however, that this indicator includes residual fringes and other systematic effects in addition to pure detector noise.
- The line peak is located by fitting a parabola to the dot cloud within $\pm 0.2 \times \text{FWHM}$ of the line center taken from the gaussfit.
- The actual peak height, line centroids and line widths are determined from the rebinned profile at heights of 80, 50, 20, 10, 5, 2, 1% of the peak, unless this probes down into regions of low S/N or is explicitly suppressed by a specification in the input file.
- Line asymmetries due to detector memory effects are searched for. Rebinned versions of down- and upscan are subtracted, causing a s-shape residue in case of memory effects. This is quantified in an asymmetry parameter which is derived by inverting the residue on one side of the line peak, and then taking the average of the entire residue over various multiples of a FWHM.
- The rebinned line profiles and derived parameters are stored in a structure ('observation structure') like

```

linestr={c321_rec,$
    ident : ident      ,\$ ; line identification (unique string)
    line  : line       ,\$ ; line tag from aar
    aotband: aotband   ,\$ ; aotband id (string)
    fcont  : fcont      ,\$ ; continuum flux [Jy]
    fline  : fline      ,\$ ; line flux [Jy]
    noise  : noise      ,\$ ; noise indicator [Jy]
    wcen   : wcen      ,\$ ; observed wavelength [micrometer]
    fwhm   : fwhm      ,\$ ; fwhm of total gaussfit [micrometer]
    efwhm  : efwhm     ,\$ ; error of fwhm
    detfwhm: detfwhm   ,\$ ; fwhm of gaussfits for 12 dets
    peak   : peak      ,\$ ; actual peak height
    center : center    ,\$ ; centers at different height
    width  : width     ,\$ ; widths at different height
    asym   : asym      ,\$ ; memory asymmetry parameter at 1-10 FWHM
    nw     : n          ,\$ ; number of wavelength points
    wave   : PTR_NEW(aaraver.data.wave) ,\$ ; wavelength
    flux   : PTR_NEW(aaraver.data.flux) ,\$ ; flux
    stdev  : PTR_NEW(aaraver.data.stdev)} ; stdev

profiles={header   : aar.header, $
          tdt      : tdt      , $
          instra   : instra   , $
          instdec  : instdec  , $
          instroll : instroll , $
          aotn    : aotn    , $
          source   : source   , $
          size     : size     , $
          sizeref  : sizeref  , $
          vwidth   : vwidth   , $
          vwidthref: vwidthref, $
          vhel    : vhel    , $
          vhelref  : vhelref  , $
          data     : replicate(linestr,ngood)}

```

6.2 Emission lines used for line profile determination

Table 6 gives an inventory of all lines used in our CAP. Of course, each individual observation will cover only a subset not only for trivial reasons of S/N and observation setup, but also since there are some blends like Brackett β / H₂(1-0)O(2) which should only be used if knowledge of the source indicates one of them to be completely dominant.

6.3 Sources used for line profile determination

Table 8 summarizes general data for all sources included up to now into the line profile database. It should be emphasized that many of the numbers should be considered best effort approximation rather than well known quantities. The spatial structure is often not well known or not easily captured into a ‘diameter’. Usually, we have tried to use a diameter in the sense of FWHM e.g. in radio continuum, not in the sense of diameter of the faintest wisps. This implies that some of our table entries differ from values tabulated in the listed references, since we tried to estimate according to our approach from figures rather than using a tabulated total diameter. Also, the source structure will differ from line to line due to effects like stratification of different ionization stages. Similar caution applies to the velocity widths, which should be understood as either the FWHM of a measured high resolution line profile, or as twice the expansion velocity catalogued for many planetary nebulae.

Line	Lambda	Ident	Cut	Range	Note
H ₂ (1-0)Q(1)	2.4066	(1-0)Q(1)			
H ₂ (1-0)Q(3)	2.4237	(1-0)Q(3)			
H 18-5	2.4700	H18-5	0.40		Blue He satellites
H 17-5	2.4953	H17-5	0.40		Blue He satellites
H 16-5	2.5261	H16-5	0.40		Blue He satellites
H 15-5	2.5643	H15-5	0.40		Blue He satellites
H ₂ (2-1)Q(1)	2.5510	(2-1)Q(1)			
H Br β	2.6259	H6-4	0.40	2.614-2.640	Blue He satellites, H ₂
H ₂ (1-0)O(2)	2.6269	(1-0)O(2)			Br β !!
H 12-5	2.7583	H12-5	0.40		Blue He satellites
H ₂ (1-0)O(3)	2.8025	(1-0)O(3)			
HeII 9-7	2.8260	HeII9-7			
H 11-5	2.8730	H11-5	0.40	2.855-2.881	Blue He satellites
H ₂ (1-0)O(4)	3.0039	(1-0)O(4)			
H 10-5	3.0392	H10-5	0.40		Blue He satellites
HeII 7-6	3.0917	HeII7-6	0.10		Red HeII 11-8 sat.
HeII 14-9	3.1455	HeII14-9	0.10	3.13-3.15	Nearby HeII 19-10
H ₂ (1-0)O(5)	3.2350	(1-0)O(5)			
H Pf δ	3.2970	H9-5	0.40		Blue He satellites, on PAH
H ₂ (2-1)O(5)	3.4379	(2-1)O(5)			
HeII 13-9	3.5443	HeII13-9			
H Pf γ	3.7406	H8-5	0.40	3.718-3.746	Blue He satellites+H17-6
H 16-6	3.8195	H16-6	0.40		Blue He satellites
H 15-6	3.9075	H15-6	0.40		Blue He satellites
H 14-6	4.0209	H14-6	0.40		Blue He satellites
H Br α	4.0523	H5-4	0.40	4.043-4.075	Blue He satellites
[Mg IV]	4.4867	Mg4_449			
[Ar VI]	4.5295	Ar6_453			
H Pf β	4.6538	H7-5	0.40		Blue He satellites
H ₂ S(9)	4.6947	S(9)			
HeII 8-7	4.7635	HeII8-7			
H 10-6	5.1287	H10-6	0.40		Blue He satellites
H ₂ S(7)	5.5112	S(7)			
[Mg V]	5.6099	Mg5_561			
H 9-6	5.9082	H9-6	0.40		Blue He satellites
H ₂ S(5)	6.9095	S(5)			
[Ar II]	6.9853	Ar2_699			
H Pf α	7.4599	H6-5	0.40	7.410-7.490	Blue He satellites
[Ne VI]	7.6524	Ne6_765			
H ₂ S(4)	8.0251	S(4)			
[Ar III]	8.9914	Ar3_899		8.940-9.035	Blended with [Mg VII]?
H ₂ S(3)	9.6649	S(3)			
[S IV]	10.5105	S4_1051			
[Cl I] H ₂ S(2)	12.2786	S(2)			
H 7-6	12.37	H7-6	0.40		Blue He satellites
[Ne II]	12.8136	Ne2_1281			
[Ar V]	13.1022	Ar5_1310			
[Mg V]	13.5213	Mg5_1352			
[Ne V]	14.3217	Ne5_1432			near [Cl III] 14.368
[Ne III]	15.5551	Ne3_1555			
H ₂ S(1)	17.0348	S(1)			
H 8-7	19.0619	H8-7	0.40		Blue He satellites
[S III]	18.7130	S3_1871			
[Ar III]	21.8293	Ar3_2183			
[Fe III]	22.9250	Fe3_2293			
[Ne V]	24.3175	Ne5_2432			
[O IV]	25.8903	O4_2589		25.75-25.96	Near [Fe II] 25.988
[Fe II]	25.9883	Fe2_2599			Near [O IV] 25.890
[S III]	33.4810	S3_3348			
[Si II]	34.8152	Si2_3481			
[Ne III]	36.0135	Ne3_3601			

Table 6: List of lines used for line profile checks. ‘Cut’ is the height below which profile parameters have never been measured, to avoid satellites. ‘Range’ denotes cases where a standard SWS02 range has to be excluded from the measurements to block nearby lines.

Line	Lambda	Reason for rejection
H 8-6	7.502	Always blended with H 11-7

Table 7: List of lines **NOT** used for line profile checks

Source	RA (J2000) HH MM SS.S	DEC (J2000) +DD MM SS	Dia arcsec	Ref (Dia)	Vwidth km/s	Ref (Vwidth)	V _{HeI} km/s	Ref (V _{HeI})
NGC 40	00 13 01.0	+72 31 19	30	ApJS 100,159	52	AAS 78,301	-20.4	AAS 132,13
IC 418	05 27 28.3	-12 41 48	12	AA 215,101	27	AA 215,101	61.0	ApJ 334,862
NGC 2022	05 42 06.3	+09 05 10	17	ApJS 100,159	52	AAS 78,301	14.0	AAS 132,13
IC 2165	06 21 42.6	-12 59 10	6	AJ 90,2055	40	AAS 78,301	53.9	AAS 132,13
IC 2501	09 38 47.5	-60 05 28	2	ApJS 14,154	35	Guess	32.7	ApJS 52,399
NGC 3918	11 50 17.2	-57 10 53	12	ApJ 314,551	48	AAS 78,301	-16.1	AAS 132,13
IC 4191	13 08 47.6	-67 38 38	20	AAS 96,23	27	AAS 78,301	-18.3	AAS 132,13
NGC 5315	13 53 57.9	-66 30 52	6	Acker 92	80	AAS 78,301	-34.5	AAS 132,13
He 2-111	14 33 19.8	-60 49 48	20	PASP 103,275	24	AAS 78,301	-10.4	AAS 132,13
NGC 5882	15 16 50.1	-45 38 59	10	AAS 96,23	37	AAS 78,301	9.7	AAS 132,13
Me 2-1	15 22 19.4	-23 37 31	5	AAS 84,229	26	AAS 78,301	44.4	AAS 132,13
NGC 6153	16 31 31.8	-40 15 15	24	Acker 92	35	AAS 78,301	38.8	AAS 132,13
NGC 6210	16 44 29.5	+23 48 00	10	AJ 109,2600	42	AAS 78,301	-36.2	AAS 132,13
IC 4634	17 01 33.8	-21 49 31	6	AAS 84,229	28	AAS 78,301	-36.3	AAS 132,13
NGC 6302	17 13 44.2	-37 06 06	8	ApJ 345,862	40	ApJ 345,862	-39.0	ApJS 52,399
NGC 6445	17 49 14.9	-20 00 40	33	Acker 92	76	AAS 78,301	16.2	AAS 132,13
NGC 6543	17 58 33.4	+66 37 59	16	AA 215,101	36	SWS-FP	-66.1	ApJS 52,399
NGC 6537	18 05 13.2	-19 50 34	6	ApJS 69,831	36	AAS 78,301	-16.9	AAS 132,13
NGC 6567	18 13 45.2	-19 04 34	8	Acker 92	37	AAS 78,301	119.3	AAS 132,13
NGC 6578	18 16 16.6	-20 27 02	9	Acker 92	35	Guess	4.4	AAS 132,13
M17	18 20 26.1	-16 10 38	Large	ApJ 332,379	20	ApJ 332,379	6.2	ApJ 332,379
NGC 6741	19 02 36.3	-00 26 47	8	AAS 96,23	44	AAS 78,301	41.3	AAS 132,13
W51 IRS2	19 23 39.9	+14 31 06	5	MNRAS 183,435	25	SWS-FP	42.1	ApJ 289,681
BD+30 3639	19 34 45.2	+30 30 59	5	MNRAS 284,815	50	AAS 78,301	-31.4	AAS 332,379
NGC 6818	19 43 58.4	-14 09 09	20	Acker 92	54	AAS 78,301	-14.1	AAS 132,13
NGC 6826	19 44 48.2	+50 31 30	20	AJ 116,360	22	AAS 78,301	-6.2	ApJS 52,399
NGC 6886	20 12 43.0	+19 59 21	6	Acker 92	40	AAS 78,301	-35.8	AAS 132,13
NGC 7009	21 04 10.8	-11 21 48	17	AA 215,101	44	AA 215,101	-46.6	ApJS 52,399
NGC 7027	21 07 01.7	+42 14 09	8	AA 251,611	36	SWS-FP	8.8	ApJS 52,399
Hu 1-2	21 33 08.1	+39 38 04	2	MNRAS 208,399	58	AAS 78,301	9.9	AAS 132,13
S140	22 19 12.0	+63 18 06	Large	AA 277,595	10	AA 277,595	-20.0	AA 277,595
Me 2-2	22 31 43.8	+48 48 04	1	AAS 84,229	20	AAS 78,301	-152.0	AAS 132,13
NGC 7662	23 25 54.0	+42 32 06	20	AJ 116,360	53	AAS 78,301	-13.2	AAS 132,13
Jupiter			38	Feuchtgruber	5	Feuchtgruber	~0	-
Saturn			16	Feuchtgruber	5	Feuchtgruber	~0	-
Uranus			3.6	Feuchtgruber	5	Feuchtgruber	~0	-
Neptune			2.2	Feuchtgruber	5	Feuchtgruber	~0	-
M-0.50-0.03	17 44 32.4	-29 22 42	40	Martin-Pintado	40	Martin-Pintado	0.	Dummy value
M+0.24+0.02	17 46 07.9	-28 43 22	40	Martin-Pintado	40	Martin-Pintado	0.	Dummy value
M+0.76-0.05	17 47 36.8	-28 18 31	40	Martin-Pintado	40	Martin-Pintado	0.	Dummy value
M+0.83-0.10	17 47 57.9	-28 16 49	40	Martin-Pintado	40	Martin-Pintado	0.	Dummy value
M+1.56-0.30	17 50 26.5	-27 45 30	40	Martin-Pintado	40	Martin-Pintado	0.	Dummy value
M+3.06+0.34	17 51 26.5	-26 08 29	40	Martin-Pintado	40	Martin-Pintado	0.	Dummy value
M+2.99-0.06	17 52 47.6	-26 24 25	40	Martin-Pintado	40	Martin-Pintado	0.	Dummy value
OPHW2	16 25 53.1	-24 19 15	40	Verstraete	10	Verstraete	0.	Dummy value
Orion 1SW	05 35 14.7	-05 23 42	30	ApJ474 L131	25	Rubin	0.	Dummy value

'Large' denotes extended regions of sometimes complex structure, with several positions observed. Tentative sizes have been assigned to each position on the basis of maps and SWS slit orientation (if available), otherwise we have used an ad hoc diameter of 40 arcsec.

Acker 92 = Strasbourg/ESO catalogue of Planetary nebulae, A. Acker et al., 1992

Martin-Pintado = J. Martin-Pintado, private communication, 1999. Approximate values less reliable than e.g. PN data!

Verstraete = L.Verstraete, private communication, 1999

Rubin = R.Rubin, private communication, 1999

Table 8: Sources considered for line profile determination. Note: For reasons of Signal-to-noise etc., not all lines and all sources enter the final database

References

- [Heckman et al. 1981] Heckman, T.M., Miley, G.K., van Breugel, W.J.M., Butcher, H.R., ApJ, 247, 403 (1981)
- [Leech et al. 1996] Leech, K. et al., ISO SWS Observer's Manual V3.0 (1996) http://www.iso.vilspa.esa.es/manuals/SWS_man/obsman.html
- [Leech et al. 1997] Leech, K. et al., SWS Instrument Data User's Manual (IDUM) V3.1 (1997) http://www.iso.vilspa.esa.es/manuals/sws_idum/
- [Lorente 1998] Lorente, R., "Spectral Resolution of SWS AOT1", internal report, 30.9.1998,
<http://www.iso.vilspa.esa.es/users/expllib/SWS/aot1www.ps.gz>
- [Persi et al. 1999] Persi P., et al., 1999, A&A, 351, 201
- [Rubin et al. 1998] Rubin R.H., Colgan S.W.J., Dufour R.J., Lord S.D. 1998, ApJ, 501, L209
- [Smits 1996] Smits, D., MNRAS, 278, 683 (1996)
- [Smits 1998] Smits, D., priv. comm. (1998)
- [Spoon et al. 1995] Spoon, H.W.W., van der Hucht,K.A., Lutz, D., "Planetary nebulae to be used as ISO-SWS Astronomical Calibration Sources", ISO 95-015 V1.0, 9.8.1995
- [SWS PV report 1996] SWS PV report, by members of the SIDT and SIST, Draft 1.0, October 9, 1996
- [Valentijn et al. 1995] Valentijn, E.A., Lutz, D., Salama, A., "ISO-SWS In Orbit Calibration Document (IOCD) 1.0", ISO-94-23, 7.6.1995
- [Valentijn et al. 1996] Valentijn, E.A., Feuchtgruber, H., Kester, D.J.M., et al., A&A, 315, L60 (1996)
- [van den Ancker et al. 1997] van den Ancker, M.E., Voors,R., Leech,K., "Grating instrumental profile and resolution", SWS internal report, 1.7.1997